NASA TR R-130

NATIONAL AERONAUTICS AND SPACE ADMINISTRATION

TECHNICAL REPORT
R-130

ANALYSIS OF THERMAL-PROTECTION SYSTEMS FOR SPACE-VEHICLE CRYOGENIC-PROPELLANT TANKS

By GEORGE R. SMOLAK, RICHARD H. KNOLL,
and LEWIS E. WALLNER

1962

For sale by the Superintendent of Documents, U.S. Government Printing Office, Washington 25, D.C. Yearly subscription, $15: foreign, $19;
single copy price varies according to size - - - - - - - - - Price 45 cents

TECHNICAL REPORT R-130

ANALYSIS OF THERMAL-PROTECTION SYSTEMS FOR SPACE-VEHICLE CRYOGENIC-PROPELLANT TANKS

By GEORGE R. SMOLAK, RICHARD H. KNOLL, and LEWIS E. WALLNER

Lewis Research Center
Cleveland, Ohio

Page Intentionally Left Blank

CONTENTS

TECHNICAL REPORT R-130

ANALYSIS OF THERMAL-PROTECTION SYSTEMS FOR SPACE-VEHICLE CRYOGENIC-PROPELLANT TANKS

By George R. Smolak, Richard H. Knoll, and Lewis E. Wallner

SUMMARY

Analytical techniques are presented that permit the calculation of heat-transfer rates with various thermal-protection systems for liquid-cryogenic-propellant tanks subjected to on-board, solar, and planetary heat fluxes. The thermal-protection systems considered include using closely spaced reflective surfaces (foils) and widely spaced reflective surfaces (shadow shields), insulation, arrangement of vehicle components, orientation with respect to radiant heating sources, and coatings for the control of solar absorptivity. The effectiveness of these thermal-protection systems in reducing propellant heating is shown both for ideal heat-transfer models and for a simplified hydrogen-oxygen terminal stage on a Mars mission.

The proper orientation of a space-vehicle cryogenic tank with respect to the Sun is one of the more beneficial methods of reducing the heating effect of solar flux.

Shadow shields can be extremely effective in reducing the propellant heating due to both solar and on-board fluxes. However, low-altitude planet orbits can result in high propellant heating rates due to planetary radiation reflected from the shields. For low-altitude orbits of more than a few days, foils appear to be desirable for all cryogenic-tank surfaces. Foils are also effective in reducing the on-board heating. A choice of shadow shields or foils cannot be made until a particular vehicle and a particular mission are chosen.

The thermal conductivity of insulation materials would have to be lower by about two orders of magnitude with no increase in density before insulation could compete with reflective surfaces for use in long-duration thermal protection of cryogenic tanks in space.

To demonstrate the application of the methods devised, thermal-protection systems are developed for a hydrogen-oxygen terminal stage for typical Mars missions.

INTRODUCTION

Cryogenic (low-temperature) liquids are among the best propellants currently available for both chemical- and nuclear-rocket stages. Presently, the highest specific impulses for chemical rockets are obtained by using hydrogen and oxygen or hydrogen and fluorine as propellants. Many proposed nuclear-rocket propulsion systems utilize hydrogen as the working fluid.

During the course of an interplanetary space mission, heat transfer to these cryogenic liquids from the Sun, planets, planet atmospheres, and from other components of the rocket vehicle is inevitable. This heating causes propellant vaporization and consequent loss by venting. Unless these losses are small, the potential advantage of using cryogenic propellants would be negated. Thus, thermal protection of the cryogenic liquid from the adverse heating environment is required.

The objectives of this report are to examine the problem of heat absorption by cryogenic propellants due to the thermal-radiation environment of space and to compare the effectiveness of various thermal-protection devices for specific applications. Aerodynamic heating of propellants during boost has already been discussed in references 1 and 2. The storage of propellants in circular satellite orbits has been treated in references 3 and 4. References 5 and 6 have examined the problem of propellant storage in the space environment away from planets. An analysis of hydrogen storage problems for a

nuclear-rocket mission to Mars or Venus was made in reference 7. The thermal-protection systems considered were reflective shields, attitude control, refrigeration, and freezing. The problem of cryogenic-propellant boiloff for hypothetical Mars and Venus trips using hydrogen and oxygen propellants has been analyzed in reference 8. The methods of reference 8 were used in reference 9 to account for the thermal-protection systems required on manned nuclear-rocket missions to Mars.

This report provides the basic methods of analysis required to predict the heat-transfer rates through various thermal-protection devices, thus facilitating the choice of a thermal-protection system for a particular application. The results presented in reference 8 were based on the analytical techniques presented herein. Where feasible, comparisons of the results of the present work with the results of other investigators have been included. Several methods of reducing propellant heating are analyzed in this report, including spacing between components of the vehicle, thermal-radiation shielding, orientation of the vehicle with respect to the Sun, and coatings. The effectiveness of these thermal-protection methods is compared for reducing both on-board and external heating from the Sun and planets. To clarify the procedure for choosing a particular thermal-protection system, the design of such systems for a hypothetical hydrogen-oxygen chemical-rocket terminal stage for Mars missions is included.

ANALYSIS

The sources of propellant heating may be either internal or external with respect to the rocket vehicle. Several methods of protection against these heat fluxes will be discussed.

HEAT SOURCES

On-board sources.—The on-board sources of heat flux are the adjacent components of the vehicle (i.e., any part of the vehicle to which the propellant will be exposed), and nuclear radiation (assuming a reactor is on board for either propulsion or auxiliary power). Heating caused by the gamma rays and neutron flux of a reactor has been investigated in reference 10. Therefore, no further treatment of nuclear-heating effects will be made herein.

Heating of cryogenic propellants due to adjacent components is caused by thermal radiation and by conduction through propellant lines and structural members. The rate of heating by radiation is approximately proportional to the difference between the fourth powers of the absolute temperatures of the adjacent component and the propellant. This can become relatively large if a low-temperature cryogenic is near a high-temperature (about room temperature or warmer) component. The rate of heat transfer per unit area by conduction is directly proportional to the product of temperature difference between adjacent components and thermal conductivity of the conductor, and inversely proportional to the length of the heat path. Heat transferred by conduction is therefore a function of the design features and detailed structural configuration of each specific vehicle and is not amenable to generalized treatment. For this reason, only heat transferred among components by radiation is considered in this report. The structural members that separate and support propellant tanks must be designed so as to ensure low rates of heat conduction. This may be done by using low-conductivity laminated stainless-steel supports, for example.

External sources.—The external sources of heat are the Sun and the planets. Heat is transferred between these sources and the cryogenic storage system by thermal radiation. The largest external heat flux encountered by a vehicle within our solar system is that which originates from the Sun. Because the planets are great distances from the Sun, it is assumed that the solar flux at the planets is represented by essentially parallel waves of electromagnetic radiation. Thus, for a unit area that is perpendicular to a radius vector from the Sun, this flux (outside planet atmospheres) is inversely proportional to the square of the distance from the Sun and is given by

$$\frac{\dot{Q}}{A}=\sigma\epsilon_S f_{S,P} T_S^4=\sigma\epsilon_S\left(\frac{r_S}{r_{S,P}}\right)^2 T_S^4 \qquad (1)$$

(See appendix A for the definition of all symbols.) For this report it was assumed that at Earth $\epsilon_S=1.0$, $r_S=2.2836\times10^9$ feet (0.6960×10^9 m), $r_{S,P}=4.90\times10^{11}$ feet (1.49×10^{11} m), and $T_S=10{,}360°$ R (5755° K). This resulted in a flux of 428 Btu per hour per square foot, which

agrees with the value in reference 11. Numerous other estimates of this flux have been published. These estimates range from about 420 to 440 Btu/(hr)(sq ft).

The heat flux that a vehicle receives from a planet results partly from planetary radiation and partly from reflected solar radiation. This planetary heat flux is given by

$$\frac{\dot{Q}}{A}=f\left[\sigma\epsilon_P T_P^4+\sigma a_P\epsilon_S\left(\frac{r_S}{r_{S,P}}\right)^2 T_S^4 z\right]=f\delta \quad (2)$$

where a is the albedo of the planet, and f is the angle factor between the planet and the body of interest. (Angle factors for a horizontal and vertical surface above a planet are given in appendix B.) The coefficient z accounts for the relative position of the body with respect to the planet (z is 1 at "noon" and 0 at "midnight"). Planetary constants are tabulated in table I. The planetary heat flux increases as the distance from a planet decreases and can be of the same order of magnitude as the solar flux. For example, a horizontal surface 100 statute miles above the sunlit Earth at noon would receive a planetary heat flux of approximately 234 Btu/(hr)(sq ft) (using the values for a_P and T_P shown in table I). Although this planetary flux becomes relatively large, it never exceeds the solar flux.

ASSUMPTIONS

As a simplification, it was assumed in many examples herein that a typical space vehicle is composed of components (payload, fuel, and perhaps an oxidant) having equal circular cross-sectional areas and arranged on a common axis. For a particular surface, it was assumed that the area receiving radiation is the same as the area emitting radiation.

It was also assumed that the vehicle components are at a constant temperature and that steady-state conditions prevail.

The effective temperature of space has been assumed equal to 0° R except where noted. Converting the estimate of galactic heat flux in reference 12 to temperature yields an effective space temperature of about 20° R (11° K). The storage of liquid hydrogen in any reasonable tank for space applications involves heat leaks of such magnitudes that the heating due to galactic flux becomes insignificant.

Absorptivities and emissivities were assumed to be total hemispherical values. Although references 13 and 14 indicate that, for engineering purposes, emissivity and absorptivity can be assumed to be equal, this assumption is generally valid only when the source of radiation and the receiver are at the same temperature. The spectral absorptivity of a surface can vary greatly with the wavelength of the incident radiation. Solar radiation (both direct and reflected) is concentrated predominantly in a region of short wavelength compared with radiation from bodies at low temperature (relative to the temperature of the Sun). Hence, the solar absorptivity of a surface is generally not equal to its emissivity.

METHODS OF REDUCING PROPELLANT HEAT ABSORPTION DUE TO ON-BOARD SOURCES

Spacing of components.—The net rate of heat absorption for a surface y exposed to direct and reflected thermal radiation from an adjacent surface x (in a vacuum environment) is given by

$$\frac{\dot{Q}}{A}=\frac{\sigma\epsilon_x f_{x,y}\alpha_y T_x^4}{1-f_{x,y}f_{y,x}(1-\alpha_x)(1-\alpha_y)}+\frac{\sigma\epsilon_y f_{x,y}f_{y,x}(1-\alpha_x)\alpha_y T_y^4}{1-f_{x,y}f_{y,x}(1-\alpha_x)(1-\alpha_y)}-\sigma\epsilon_y T_y^4 \quad (3)$$

where $f_{x,y}$ and $f_{y,x}$ are the angle factors ($f_{x,y}$ is the fraction of the total radiation that leaves the first surface x and arrives at the second surface y) between the two adjacent components, and T_x and T_y are the absolute temperatures of the components. This equation allows for an infinite number of diffuse reflections between components. The general method of treating these reflections is given in appendix C.

The heat absorbed by component y can be reduced by changing the emissivity and/or the absorptivity of surfaces x and y. The heat-transfer rate through surface y (for large values of $f_{x,y}$ and $f_{y,x}$) can be decreased by reducing both ϵ_y and ϵ_x. This effect will be demonstrated in the RESULTS AND DISCUSSION. Also, the net heat-absorption rate can be reduced by reducing the angle factors $f_{x,y}$ and $f_{y,x}$. By assuming that absorptivity and emissivity are equal and constant and noting that $f_{x,y}$ and $f_{y,x}$ are equal for parallel

equal-diameter circular disks (arranged on a common axis), equation (3) becomes

$$\frac{\dot{Q}}{A}=\frac{\sigma\epsilon_x f\epsilon_y T_x^4}{1-f^2(1-\epsilon_x)(1-\epsilon_y)}+\frac{\sigma\epsilon_y f^2(1-\epsilon_x)\epsilon_y T_y^4}{1-f^2(1-\epsilon_x)(1-\epsilon_y)}-\sigma\epsilon_y T_y^4 \quad (4)$$

The angle factor f between the parallel ends of the components is a function of the distance between components and their diameters. For a constant diameter, the angle factor between adjacent components will approach zero as the distance between components increases and will approach 1 as the distance decreases. When the components are separated by a large enough distance so that the angle factor is essentially zero, equation (4) becomes

$$\frac{\dot{Q}}{A}=-\sigma\epsilon_y T_y^4 \quad (5)$$

Here the body concerned loses heat to space, which has been assumed to be at 0° R.

When the components are close enough together that the angle factor is essentially equal to 1, equation (4) becomes

$$\frac{\dot{Q}}{A}=\frac{\sigma(T_x^4-T_y^4)}{\frac{1}{\epsilon_y}+\frac{1}{\epsilon_x}-1} \quad (6)$$

This is the maximum rate of heat transfer between the two components. Here it is apparent that the heat-absorption rate can be reduced by reducing either or both ϵ_y and ϵ_x. For this case the net rate of heat absorption by surface y is the same as the net rate of heat emission by surface x, because the angle factor equals 1 (i.e., no heat loss at the edges).

Thus, it appears that the heat flux from on-board sources can be decreased by increasing the distance between components. However, when propellants are subjected to radiation from external sources as well as on-board heat flux, increasing the distance between components may not be desirable. This will be discussed later.

Reflective shields.—The heat transfer between adjacent components can be greatly reduced by inserting parallel, thermally isolated, reflective shields between components as shown in sketch (a). The relation for the net rate of heat absorption by surface y with one reflective shield placed directly between the components is given by appendix D as

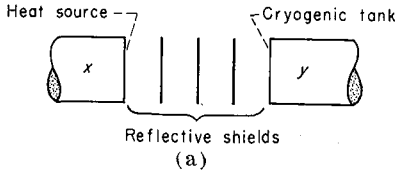

(a)

$$\frac{\dot{Q}}{A}=\frac{\sigma(\epsilon_x^2\alpha_y^2 f^2 T_x^4+\alpha_y\alpha_x\epsilon_y\epsilon_x f^2 T_y^4)}{[1-f^2(1-\alpha_y)(1-\alpha_x)][\epsilon_y(1+\alpha_x f^2-f^2)+\epsilon_x(1+\alpha_y f^2-f^2)]}-\frac{\sigma\epsilon_y(1+\alpha_x f^2-f^2)T_y^4}{[1-f^2(1-\alpha_y)(1-\alpha_x)]} \quad (7)$$

It is assumed that the reflective shield is thin enough that no temperature gradient exists across the shield. Here the angle factor f is common throughout because the shield has the same cross-sectional area as the components and is equally spaced between them. The net rate of heat absorption by surface y can be decreased by decreasing α_y and ϵ_x and by decreasing the angle factor f. The angle factor can be decreased by increasing the distance between the components and the shield. Again, when the spacing is such that f is essentially zero, equation (5) results. When the reflective shields between the components are so closely spaced that the angle factor is essentially equal to 1, the net rate of heat absorption by surface y is given by equation (D3) or

$$\frac{\dot{Q}}{A}=\frac{\sigma\epsilon_y\left[\left(\frac{\alpha}{\epsilon}\right)_y\left(\frac{\epsilon}{\alpha}\right)_x\right]^{N+1}T_x^4-\sigma\epsilon_y T_y^4}{\left(1-\alpha_y+\frac{\alpha_y}{\alpha_x}\right)\left\{\frac{1-\left[\left(\frac{\alpha}{\epsilon}\right)_y\left(\frac{\epsilon}{\alpha}\right)_x\right]^{N+1}}{1-\left(\frac{\alpha}{\epsilon}\right)_y\left(\frac{\epsilon}{\alpha}\right)_x}\right\}} \quad (8)$$

The equations for the net rate of heat absorption by surface y with 2, 3, . . ., N shields between components are given in appendix D. In general, the heat-absorption rates can be decreased by increasing the number of shields. Hereinafter, the widely spaced shields will be referred to as shadow shields, and the closely spaced shields ($f=1$) will be referred to as foils.

When $(\alpha/\epsilon)_y(\epsilon/\alpha)_x=1$, in equation (8), the term $\{1-[(\alpha/\epsilon)_y(\epsilon/\alpha)_x]^{N+1}\}/[1-(\alpha/\epsilon)_y(\epsilon/\alpha)_x]$ should be

replaced by $(N+1)$. Then, if $\alpha_x=\epsilon_x$ and $\alpha_y=\epsilon_y$, equation (8) becomes

$$\frac{\dot{Q}}{A}=\frac{\sigma(T_x^4-T_y^4)}{\left(\frac{1}{\epsilon_y}+\frac{1}{\epsilon_x}-1\right)(N+1)} \tag{9}$$

From this equation it is apparent that the heat-transfer rate can be reduced by increasing the number of foils or decreasing the emissivity of the components. Thus, the heat-absorption rate of a surface y can be reduced considerably by placing shadow shields or foils between it and the adjacent component.

Insulation.—Another means of reducing the heat transfer between components is to use insulation in this area. The best available purely insulative materials have such a high thermal conductivity that they are unattractive on a weight basis compared with multiple reflective surface materials for the protection of cryogenic propellant tanks in the environment of space. It was shown in reference 8 that the thermal conductivity of insulation materials would have to be lower by about two orders of magnitude (from a current low value of about 0.001 (Btu)(in.)/(hr)(sq ft)(°F)) with no increase in density before insulations could compete with reflective surfaces for use in long-duration thermal protection of cryogenic tanks in space. It is recognized, however, that insulation may be used extensively both for protection against aerodynamic heating and for protection of noncryogenic-propellant tanks in space.

METHODS OF REDUCING PROPELLANT HEAT ABSORPTION DUE TO EXTERNAL HEAT SOURCES

The techniques of reducing propellant heat absorption due to internal heat sources were restricted to those encountered in normal ground installations. When the propellant tank is assumed to be in space, the external radiation environment and concomitant methods of reducing propellant heat absorption differ in some respects from those previously discussed. The methods that will be discussed are (1) using coatings having a low absorptivity for the incident radiation, (2) using reflective surfaces, and (3) varying the orientation of the propellant tank with respect to the incident radiation.

Coatings.—If it is assumed, as shown in sketch (b), that flux Y is incident upon an element of

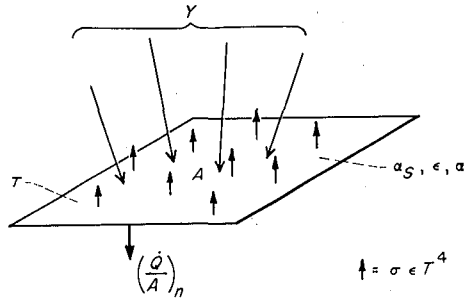

(b)

surface area A having an absorptivity α, a solar absorptivity α_S, an emissivity ϵ, and a temperature T, then the net rate of heat transfer through the surface is, in general,

$$\left(\frac{\dot{Q}}{A}\right)_n=\alpha Y-\sigma\epsilon T^4 \tag{10}$$

For the special case where Y is direct solar flux or planetary flux (due to albedo and planet temperature), equation (10) becomes

$$\left(\frac{\dot{Q}}{A}\right)_n=\alpha_S Y-\sigma\epsilon T^4 \tag{11}$$

In general, if Y is from a body at a temperature less than the melting point of common metals, then $\alpha=\epsilon$. If Y is from the Sun, $\alpha_S\neq\epsilon$, and α_S/ϵ may be less than or greater than unity depending on the composition of surface A. For problems involving storage of propellants near the Earth, Y_{max} is about 428 Btu/(hr)(sq ft). In order to minimize $(\dot{Q}/A)_n$, a material or coating having low α_S and high ϵ should be used. For silica oxide on magnesium, reference 15 gives $\alpha_S=0.21$ and $\epsilon=0.83$. Therefore, in order for the T^4 term to be significant (say 1 percent as large as the Y term), T must be greater than about 160° R (89° K). Thus, coatings for bare cryogenic tanks should have mainly low values of α_S, but coatings for higher temperature surfaces (e.g., the outermost surface of insulations) should have not only a low value of α_S but also a high value of ϵ.

It has been shown previously that the rate of heat absorption by a surface in space subjected to solar flux is strongly dependent upon the values of solar absorptivity and emissivity peculiar to the surface. Some control of these properties is possible through the use of coatings (paints, oxides, metals, etc.). However, as shown in

reference 16, the solar absorptivity and emissivity may change significantly after exposure to ascent heating, Van Allen radiation, sputtering, meteoroid erosion, the ultraviolet component of solar radiation, and prelaunch oxidation and corrosion.

Emissivity values may range from 0.02 to about 0.9, and solar absorptivity to emissivity ratios may range from about 0.2 to 21 (refs. 15 to 17). For most space missions there would undoubtedly be an optimum coating or material to use for each particular surface of a vehicle. To indicate such optimums is beyond the scope of this report. The analytical relations included in this report have in most cases included solar absorptivity as a parameter.

In view of the fact that long-duration exposure of surfaces to the space environment may alter surface solar absorptivity and emissivity (ref. 16), conservative assumptions for surface properties have been assumed herein. To suggest at this time using extremely low values for α_S or ϵ for long space missions would involve considerable risk of change in these surface properties during the mission.

Reflective shields.—One method of reducing the heat transfer into an exposed cryogenic-tank surface is to place shadow shields between the cryogenic surface and the external heat source as shown in sketch (c). When the incoming waves of electromagnetic radiation are incident only on the outer surface of the outermost shield, the expression for the net rate of heat absorption by surface y with one shadow shield placed between it and the external flux Y is given by

$$\frac{\dot{Q}}{A}=\frac{\alpha_S\epsilon_x\alpha_y fY}{[1-f^2(1-\alpha_x)(1-\alpha_y)](\epsilon_o+\epsilon_x)-\epsilon_x f^2(1-\alpha_y)\alpha_x}+\frac{\sigma\alpha_y\alpha_x\epsilon_y\epsilon_x f^2T_y^4}{[1-f^2(1-\alpha_y)(1-\alpha_x)]\times\{[1-f^2(1-\alpha_y)(1-\alpha_x)](\epsilon_o+\epsilon_x)-\epsilon_x f^2(1-\alpha_y)\alpha_x\}}+\frac{\sigma\epsilon_y f^2(1-\alpha_x)\alpha_y T_y^4}{[1-f^2(1-\alpha_y)(1-\alpha_x)]}-\sigma\epsilon_y T_y^4 \quad (12)$$

where $\alpha_S Y$ is the fraction of incident solar and/or planetary radiation absorbed by the surface exposed to flux Y, ϵ_o is the emissivity (absorptivity) of all other shield surfaces, and α_y and ϵ_y are the absorptivity and emissivity, respectively, of the

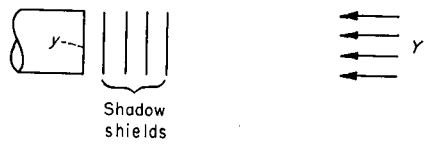

(c)

tank surface y. The angle factor f is common throughout because the cross-sectional areas of the cryogenic-tank surface and the shadow shield were assumed to be equal. (The equation for unequal cross-sectional areas can be developed with the techniques presented in appendixes C and D.) Again, when the angle factor approaches zero, equation (5) results. It is also apparent from equation (12) that the net heat-absorption rate of surface y can be reduced by decreasing α_S and/or increasing ϵ_o. The equations for 2, 3, . . ., N shadow shields are presented in appendix D. In general, the heat-absorption rate can be decreased by increasing the number of shadow shields. If it had been assumed that the shadow shields had a finite thermal conductivity laterally, a temperature gradient would have existed in the lateral direction. It is conceivable that this temperature gradient could be important if a more exact calculation of shield temperature is required. Analytical techniques for determining this temperature gradient are shown in reference 18.

The heat-absorption rate of a cryogenic-tank surface exposed to an external flux can also be reduced by applying foils as shown in sketch (d).

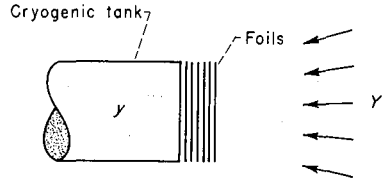

(d)

This case is the same as the shadow-shield case represented by equation (12), except that, with foils, the angle factor between adjacent surfaces has a value of 1.

The relation for the net heat-absorption rate of surface y with N foils protecting it can be derived from equation (12) and is given by equation (D8) or

$$\frac{\dot{Q}}{A}=\frac{\frac{\alpha_S}{\epsilon_o}\left[\left(\frac{\alpha}{\epsilon}\right)_y\left(\frac{\epsilon}{\alpha}\right)_x\right]^N \epsilon_y Y-\sigma\epsilon_y T_y^4}{\left(1-\alpha_y+\frac{\alpha_y}{\alpha_x}\right)\left\{\frac{1-\left[\left(\frac{\alpha}{\epsilon}\right)_y\left(\frac{\epsilon}{\alpha}\right)_x\right]^N}{1-\left(\frac{\alpha}{\epsilon}\right)_y\left(\frac{\epsilon}{\alpha}\right)_x}\right\}+\frac{\epsilon_y}{\epsilon_o}\left[\left(\frac{\alpha}{\epsilon}\right)_y\left(\frac{\epsilon}{\alpha}\right)_x\right]^N} \tag{13}$$

When $(\alpha/\epsilon)_y(\epsilon/\alpha)_x=1$, the term $\{1-[(\alpha/\epsilon)_y(\epsilon/\alpha)_x]^N\}/[1-(\alpha/\epsilon)_y(\epsilon/\alpha)_x]$ should be replaced by N. Then, by assuming that $\alpha_y=\epsilon_y$ and $\alpha_x=\epsilon_x$, equation (13) becomes

$$\frac{\dot{Q}}{A}=\frac{\alpha_S Y-\sigma\epsilon_o T_y^4}{\epsilon_o\left(\frac{1}{\epsilon_y}+\frac{1}{\epsilon_x}-1\right)N+1} \tag{14}$$

which is identical to a relation presented (but not derived) in reference 5. Thus, the net rate of heat absorption of incident radiation Y by a cryogenic-tank surface y can be reduced by increasing the number of foils, decreasing the emissivities of the inner foils (ϵ_y, ϵ_x), decreasing the solar absorptivity of the exposed outer surface (α_S), and/or increasing the emissivity of the outer surface (ϵ_o).

Appendix D gives equations that predict the rate of heat transfer when combinations of the preceding shielding devices are utilized.

Orientation.—For any body in space, the amount of heat absorbed from solar flux or planetary flux depends on the area exposed to these radiant heat sources. The amount of solar heat absorbed can be minimized by minimizing the projected area exposed to the Sun. Thus, for the vehicles shown in figure 1, the incident solar flux will be minimized by alining the longitudinal axis of the stage with the position vector of the stage relative to the Sun. At the extremely great distances from the Sun of concern here, the solar flux is nearly parallel. Thus, the sides of the vehicle essentially will not "see" the Sun. For space-vehicle operation in the vicinity of either the Sun or a planet, the apparent flux is not parallel. Therefore, while vehicle orientation can minimize the projected area, it cannot completely eliminate the heating effect of this flux.

RESULTS AND DISCUSSION

Two space vehicles of current interest that use cryogenic propellants are (1) the high-specific-impulse chemical rocket (with liquid hydrogen as the fuel and liquid oxygen or liquid fluorine as an oxidizer), and (2) the nuclear rocket (with liquid hydrogen as the fuel). Schematic diagrams of these vehicles are shown in figure 1. Each vehicle has a payload, a propellant (or propellants), and an engine. It was assumed that the cross-sectional areas of the components were circular and that the propellant tanks were cylindrical. It was also assumed that the payload temperature was 520° R (290° K) and that the propellants, hydrogen and oxygen, for example, were slightly subcooled, having constant temperatures of 30° and 140° R (17° and 78° K), respectively. Liquid oxygen was selected as the chemical-rocket oxidant merely for purposes of discussion. Fluorine could also have been used, as its storage temperature and vaporization characteristics are similar to those of oxygen. With the basic components of these two vehicles defined, it is now possible to examine the various thermal-protection techniques suggested in the ANALYSIS. These thermal-protection techniques are not limited to the vehicles chosen, but are applicable for any space storage system.

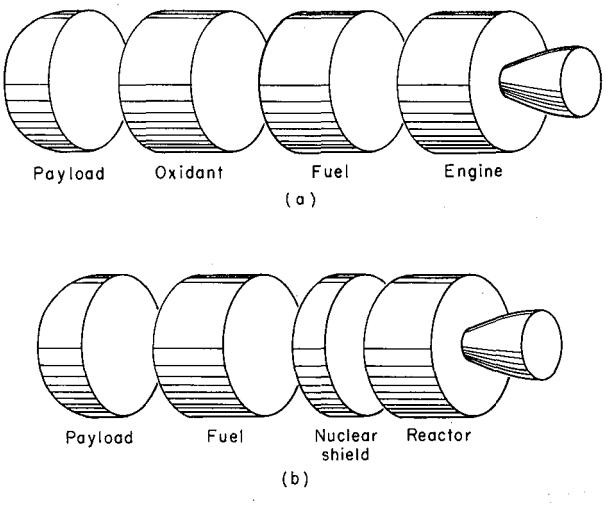

(a) Typical chemical-rocket stage.
(b) Typical nuclear-rocket stage.

FIGURE 1.—Schematic diagrams of rocket stages.

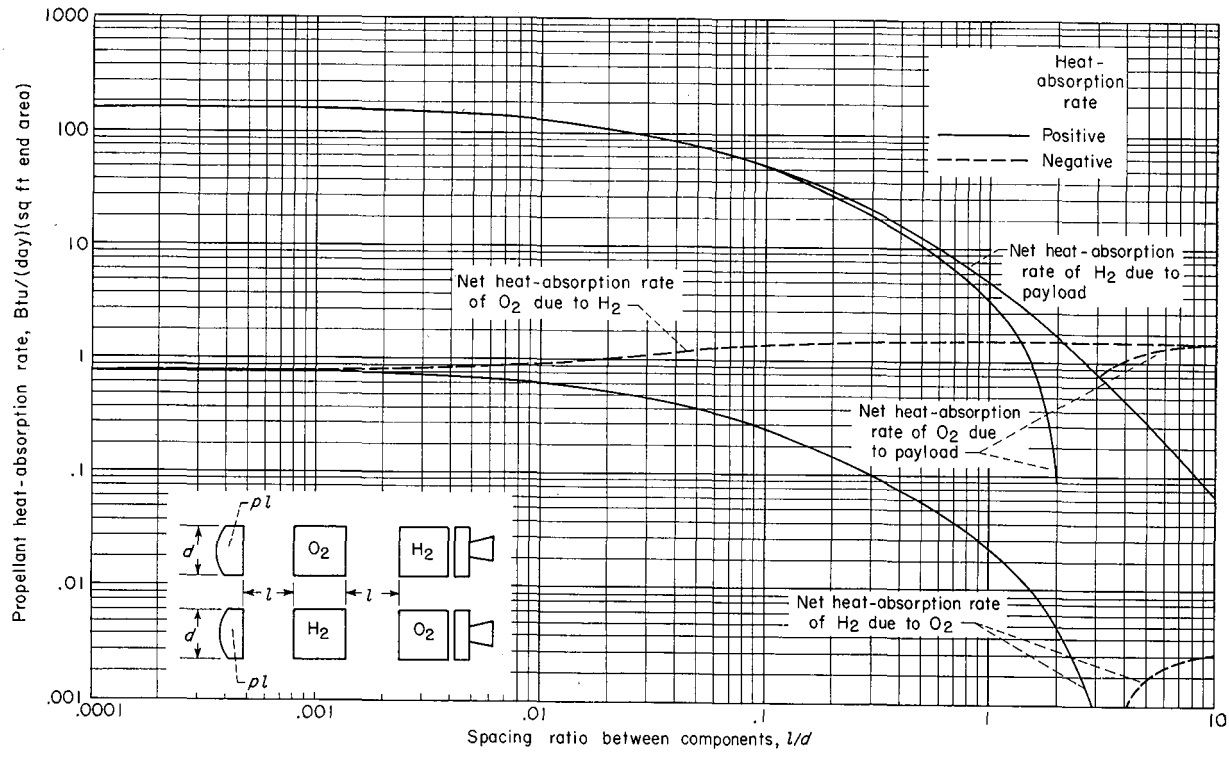

FIGURE 2.—Effect of arrangement and spacing of vehicle components on propellant heat-absorption rate ($\alpha=\epsilon=0.1$).

THERMAL PROTECTION AGAINST ON-BOARD HEATING

Arrangement and spacing of vehicle components.—The basic arrangement and spacing of the various components of any vehicle utilizing cryogenic propellants can have profound effects upon the thermal-protection problem. In figure 2, the propellant heating rate is plotted against the spacing ratio between various components for a constant value of absorptivity and emissivity ($\alpha=\epsilon=0.1$).[1] For this figure it was assumed that there was heat transfer only between components (i.e., there was no heat transfer through the sides of the cryogenic containers.) The effectiveness of spacing in reducing heat transfer between components includes the external effect that the tank ends are allowed to radiate to space. Negative heat-absorption rates indicated here and on other figures in this report signify a net loss from a particular surface. It is evident that the heating rates vary widely, depending on the temperature of the adjacent component. For example, the heat-absorption rate of hydrogen when placed next to a 520° R payload is 160 Btu/(day)(sq ft), and when placed next to an oxygen tank is 0.83 Btu/(day)(sq ft) (assuming $l/d=0.0001$). Assuming $l/d=0.0001$ between all components and that the components are arranged in descending order of temperature (top sketch in fig. 2), the net hydrogen heat-absorption rate is 0.83 Btu/(day)(sq ft) (radiation from hydrogen to space is negligible compared with 0.83 Btu/(day)(sq ft) from oxygen). The net oxygen heat-absorption rate for this configuration (160 Btu/(day)(sq ft)) is a result of heating on the payload end (160 Btu/(day)(sq ft)) and cooling on the hydrogen end (0.83 Btu/(day)(sq ft)). By interchanging the propellant tanks (lower sketch in fig. 2), the hydrogen heat-absorption rate is 160 Btu/(day)(sq ft), and the oxygen cooling rate is 0.83 Btu/(day)(sq ft). The optimum arrangement of components depends not only on the magnitude of these rates but also on the absolute size and shape of the propellant tanks, the fluid configuration within the tanks, and the effectiveness of other protection devices in reducing on-board flux. Another point that should be emphasized here is that the optimum arrangement of components will also depend upon the mission profile (i.e.,

[1] Absorptivities and emissivities of the order of 0.1 are typical of oxidized aluminum, polished stainless steel, and smooth unpolished monel (refs. 14 and 19).

the external heat sources and their temporal variation will have some bearing on the arrangement of components.)

It is also apparent from figure 2 that the heat-absorption rates can be decreased considerably by increasing the spacing ratio. For example, the heat-absorption rate of hydrogen due to heat transfer from the payload can be reduced from 160 to 0.1 Btu/(day)(sq ft) merely by increasing l/d from 0.0001 to 8.6. Increased spacing ratios have the adverse effect of increasing the structural weight.

Shadow shielding.—Figure 3 demonstrates how shadow shields may be used to reduce on-board heat flux. In figure 3(a) the heat-absorption rate of hydrogen when placed adjacent to a 520° R source of heat is plotted against the number of shadow shields between the tanks. Several values of spacing ratio between adjacent surfaces are shown. Emissivity and absorptivity are assumed equal to 0.1. For this figure and for several others throughout this report, curves are shown even though data are valid only for integer values of reflective surfaces. From the figure it is apparent that shadow shields are capable of reducing the heat transfer between tanks considerably. For any given number of shadow shields, the heat-absorption rate decreases with increasing spacing ratio l/d. With extremely small l/d, the angle factor between adjacent shields approaches 1. Thus, the shadow shield and foil equations should be expected to yield nearly the same value. Figure 3(a) shows this effect for small numbers of shields. For all values of l/d, if a large enough number of shadow shields is used, the hydrogen heat-absorption rate eventually becomes negative because of radiation to space from the shield and tank surfaces. For example, if the l/d between adjacent surfaces is 0.01, the hydrogen heat-absorption rate is negative for 14 or more shadow shields spaced between the 520° R heat source and the 30° R hydrogen. Also, if the l/d is 1, the heat-absorption rate is negative even for two shields between the components.

In figure 3(b), the propellant heat-absorption rate is plotted against the number of shadow

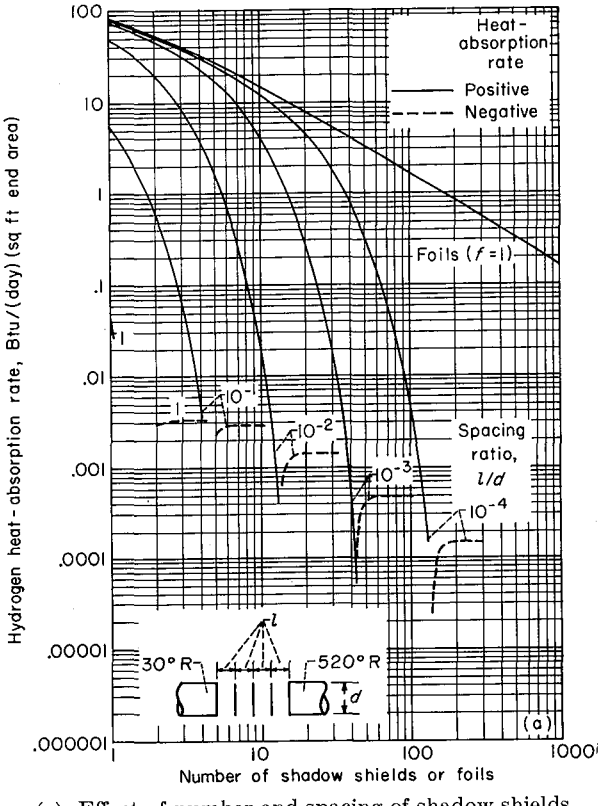

(a) Effect of number and spacing of shadow shields ($\alpha = \epsilon = 0.1$).

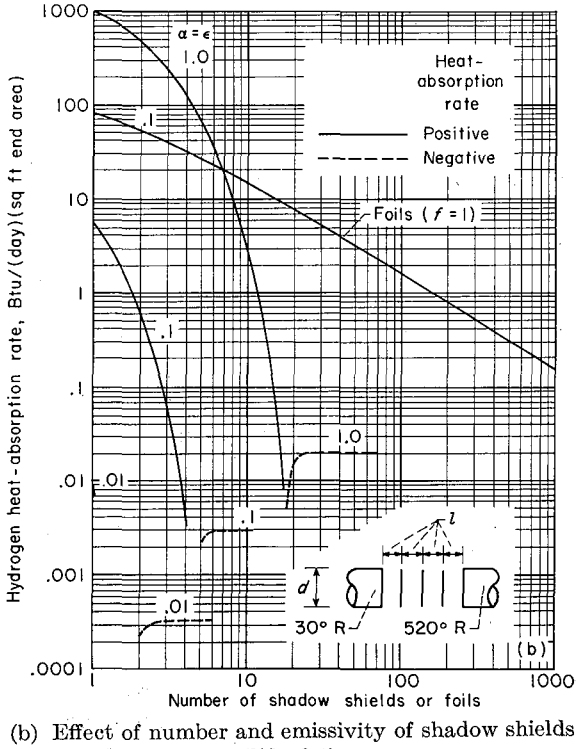

(b) Effect of number and emissivity of shadow shields ($l/d = 0.1$).

FIGURE 3.—Shadow shields for reducing on-board heating effects.

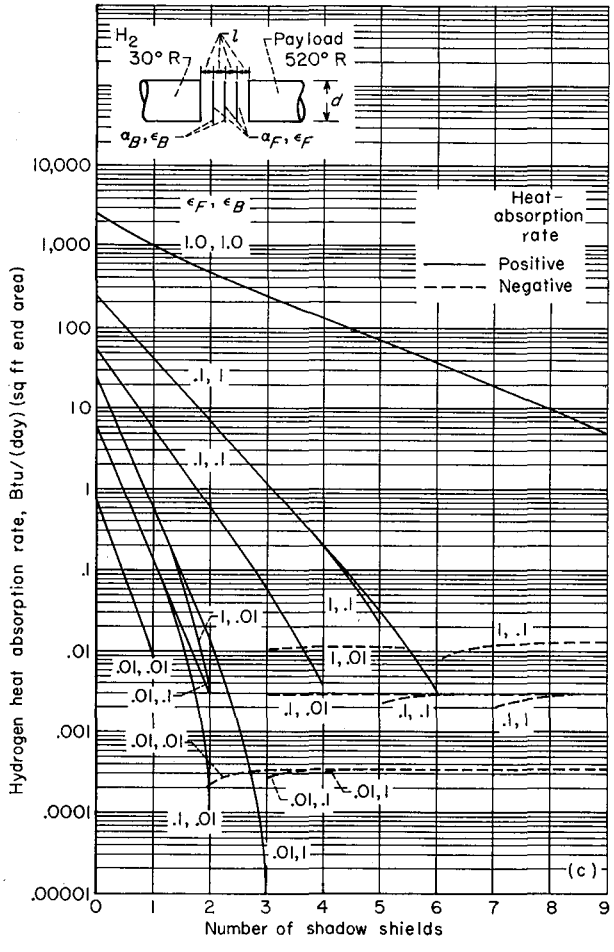

(c) Effect of number of shadow shields and variation of emissivity from front ($l/d=0.1$; $\alpha_B=\epsilon_B$; $\alpha_F=\epsilon_F$).

FIGURE 3.—Concluded. Shadow shields for reducing on-board heating effects.

shields for a range of emissivities using a constant value of spacing ratio l/d of 0.1. Decreased heat-absorption rates are obtained by decreasing the emissivity or increasing the number of shadow shields, or both.

Figure 3(c) is included to show the effect of both the number of shadow shields and the variation of shield emissivities from front to back surfaces on the hydrogen heat-absorption rate. In each case, the spacing ratio between reflective surfaces was assumed to be 0.1. Emissivity and absorptivity on a particular surface were assumed to be equal (see ANALYSIS). The figure indicates that decreases in emissivity on any surface will result in lower heat-absorption rates. The lowest absorption rates are obtained by using the lowest value of absorptivity and emissivity on all surfaces. For figure 3(c) it appears that decreasing the value of ϵ_B is more effective in reducing the hydrogen heat-absorption rate than decreasing the value of ϵ_F. Data from references 14 and 19 indicate that the emissivity of aluminum can conservatively be taken as 0.1. Optimistically, emissivity values as low as 0.01 may be found for certain silver or aluminum surfaces.

Foils.—By laminating alternate layers of aluminum foil and glass-fiber paper (as described in ref. 20), heat-transfer characteristics are attainable that approximate those of foils. Laminated assemblies of this type weigh only about 0.01 pound per square foot per foil and contain about 50 foils per inch of thickness. Figure 4 shows the effect of the number of foils on the hydrogen heat-absorption rate due to heat transfer between hydrogen, oxygen, and a payload. Emissivity levels of 1.0, 0.1, and 0.01 are shown (the 0.1 value yielding heat-absorption rates conservatively approximating commercial foils, refs. 20 to 22). It was

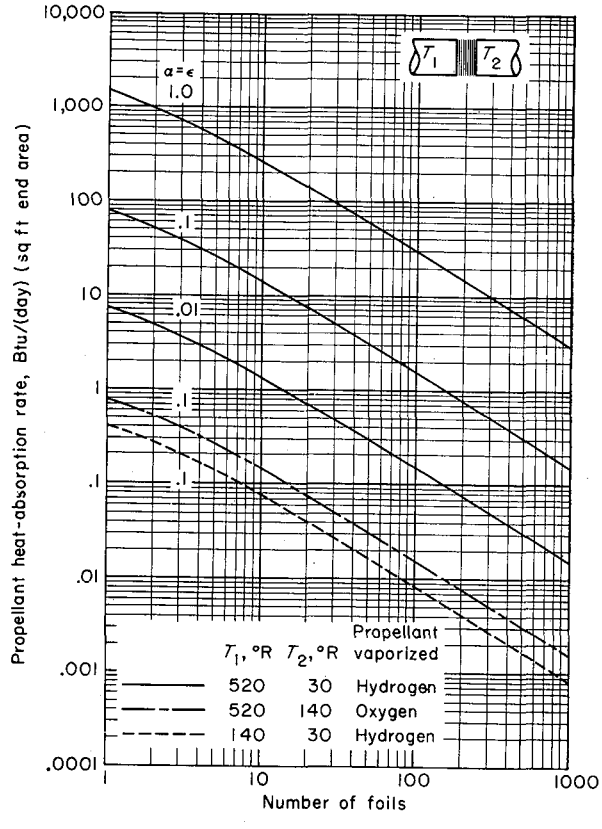

FIGURE 4.—Effect of number and emissivity of foils in reducing on-board heating.

assumed that emissivity and absorptivity are equal. Increasing the number of foils and decreasing the foil emissivity both decrease the rate of heat absorption. It is apparent from the figure that the heat-absorption rate due to placing hydrogen adjacent to a 520° R heat source is much larger than the hydrogen heat-absorption rate due to hydrogen and oxygen tanks being adjacent. For example, if $\alpha=\epsilon=0.1$, and if 100 foils are used for protection, the hydrogen heat-absorption rate due to a 520° R payload is about 1.6 Btu/(day)(sq ft), while the hydrogen heat-absorption rate due to a 140° R oxygen tank is only about 0.0082 Btu/(day)(sq ft).

Comparison of methods.—The choice of a particular method of achieving acceptable boiloff losses due to on-board heat flux between components is usually made on the basis of weight. Several elements of this weight problem are the weight of the protection device, the structural weight penalty necessary to employ the protection device, and the integrated weight of the propellant boiloff for the complete mission. The weight of individual shadow shields should be roughly the same as the weight of individual foils; however, additional structural-support weight will be required to span the gap between shadow shields. Structural weights for these applications are greatly dependent on both the absolute weight of the structure and the acceleration loads to which the structure will be subjected. The weight of these structures can vary from light inflatable structures to the heavy structures found between lower stages of multistage vehicles. Thus, the structural weight problem must also be defined for each particular application before a final optimization of the thermal-protection system can be made.

The hydrogen heat-absorption rate is plotted against the spacing ratio between hydrogen and an adjacent 520° R component in figure 5. For spacing ratios greater than about 0.1, the heat-absorption rate decreases rapidly with increasing l/d. Horizontal dashed lines are included in the figure to facilitate a comparison between gaps and foils for this intercomponent protection. If it is assumed that foil densities of 40 per inch are available, then 100 foils would occupy only about 2.5 inches of thickness. This number of foils would supply the same protection as components with no foils but separated by a gap of about

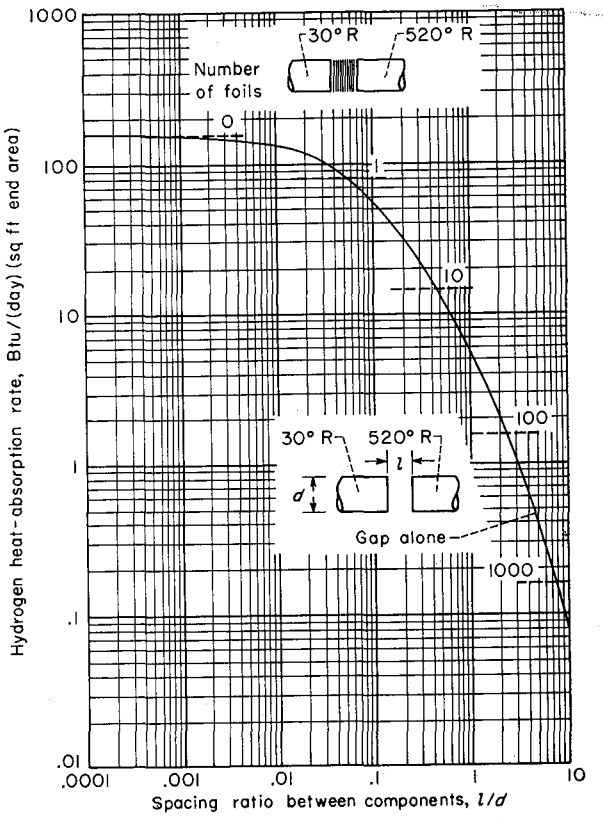

FIGURE 5.—Comparison of gaps and foils for intercomponent thermal protection ($\alpha=\epsilon=0.1$).

2.3 diameters. With intercomponent structural weights rather substantial compared with foil weights of 7 pounds per cubic foot, the use of foils would thus provide a lightweight, compact protection scheme for a heat-absorption rate of about 1.6 Btu/(day)(sq ft).

THERMAL PROTECTION AGAINST SOLAR HEATING

With fixed values of solar absorptivity and emissivity of surfaces exposed to solar flux, there remain several methods for reducing the heating effect of solar flux. These include using shadow shields, foils, and vehicle orientation with respect to the solar flux.

Shadow shields.—The effect of the number and spacing of shadow shields on the heat-absorption rate of hydrogen due to solar flux at the Earth's distance from the Sun is shown in figure 6. Emissivity and absorptivity were assumed equal to 0.1. It was also assumed that the shadow shields were alined normal to the solar radiation. The figure shows that the heat-absorption rates can be

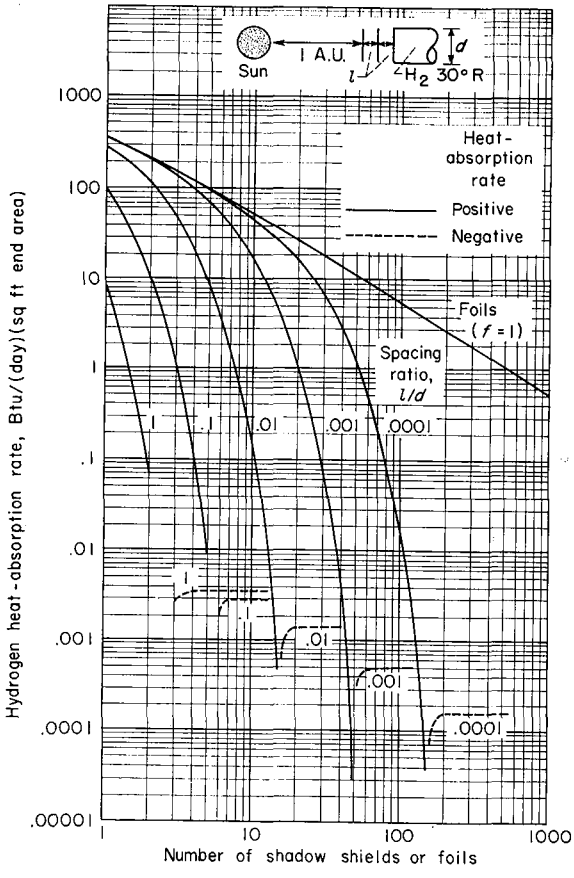

FIGURE 6.—Effect of number of foils and number and spacing of shadow shields on hydrogen heat-absorption rate due to solar flux ($\alpha_S=\alpha=\epsilon=0.1$).

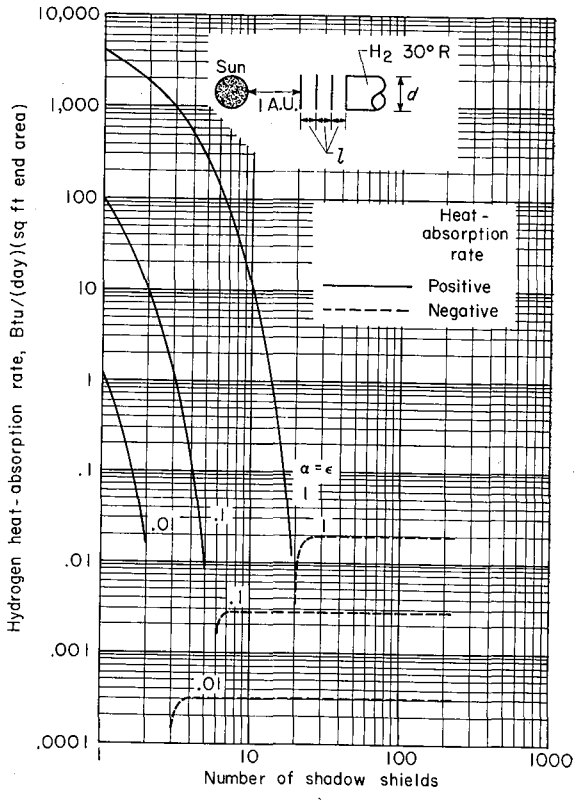

FIGURE 7.—Effect of number and emissivity of shadow shields on hydrogen heat-absorption rate due to solar flux ($l/d=0.1$).

decreased by increasing the number of shadow shields or by increasing the spacing ratio between shields.[2] For an extremely small spacing ratio between shields (≤ 0.0001), the shadow-shield and foil theories predict about the same absorption rate as for 10 foils or less. This figure also shows that, for a given spacing ratio between shields, there is a number of shields beyond which the negative heat-absorption rate is essentially constant. Hydrogen heat-absorption rates with emissivities and absorptivities from 0.01 to 1 are plotted in figure 7 against the number of shadow shields for a fixed spacing ratio between shields. Either decreasing the shadow-shield emissivity or increasing the number of shadow shields decreases the heat-absorption rate. It is interesting to note that the absorption rates for a particular l/d can be decreased by one to three orders of magnitude by decreasing the emissivity one order of magnitude. For example, the absorption rate using four shields with $\alpha=\epsilon=1$ is approximately 540 Btu/(day)(sq ft), but the absorption rate for four shields with $\alpha=\epsilon=0.1$ is only about 0.1 Btu/(day)(sq ft).

A possible shadow-shield structure would consist of rings supporting the edges of each shadow shield. Longitudinal members between components would support these rings and act as load-carrying members.

Foils.—The effectiveness of using foils for protection against solar heating is shown in figure 8. The heat-absorption rate for a hydrogen-tank end surface exposed to solar radiation at the Earth's distance from the Sun is shown against the number of foils for constant values of emissivity. Emissivity and absorptivity were assumed to be equal. The absorption rate can be decreased by either decreasing the foil emissivity or increasing the number of foils.

[2] The similarity between figs. 3(a) (shadow shields between components) and 6 (shadow shields facing Sun) is due to the similarity of the heat-transfer models. Fig. 3(a) would result for a system of shadow shields facing the Sun if the temperature of the Sun shield were 520° R.

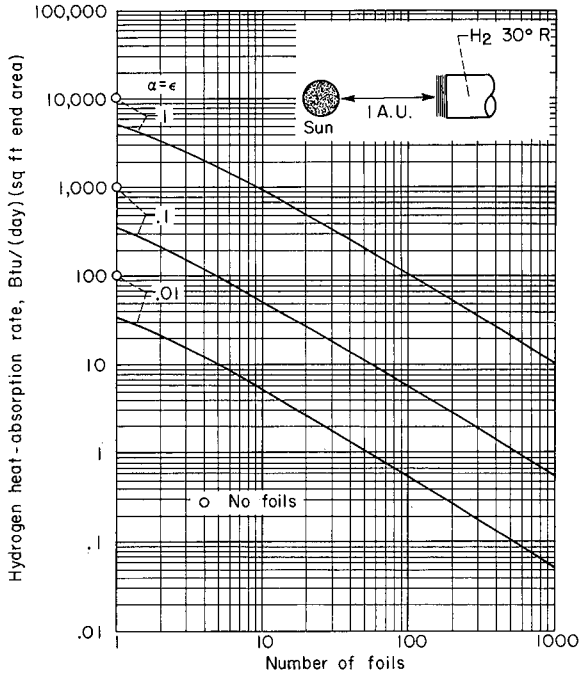

FIGURE 8.—Effect of number and emissivity of foils on hydrogen heat-absorption rate due to solar flux.

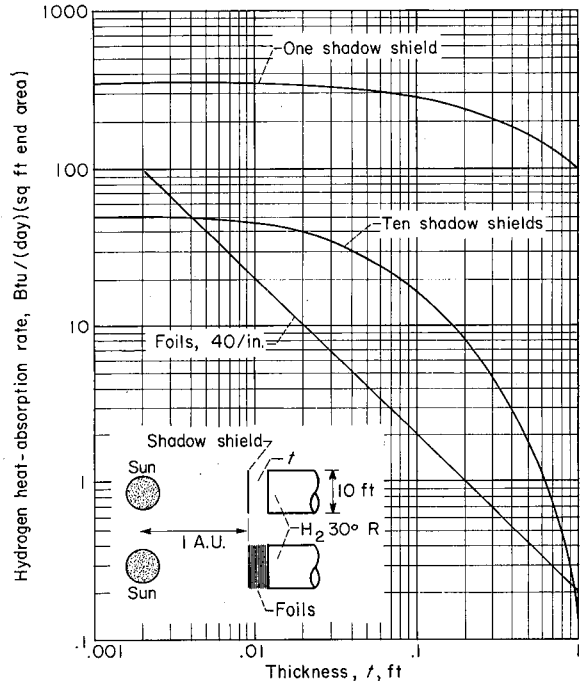

FIGURE 9.—Comparison of protection devices against solar heating on a thickness basis ($\alpha=\epsilon=0.1$).

Vehicle orientation.—One of the most obvious methods of protecting a cryogenic-tank surface from heating by solar radiation is to orient the stage so that one portion of the stage is used to cast a shadow on the cryogenic-tank surfaces. An attitude control system would be required to provide for proper orientation of the vehicle throughout the mission. However, an orientation system would probably be required anyway for such functions as attitude control of the vehicle prior to making propulsive maneuvers.

Comparison of methods.—Figure 9 compares shadow shields and foils for protecting a hydrogen tank from direct solar radiation at the Earth's distance from the Sun assuming $\alpha=\epsilon=0.1$. Hydrogen heat-absorption rate is plotted against the thickness occupied by the protection device. A specific tank diameter has been chosen for the shadow-shield data, because the vaporization rate is dependent upon the angle factor between adjacent shields, which is a function of both the spacing between shields and the shield diameter. For a given thickness, ten shadow shields provide much lower absorption rates than one shadow shield. For thicknesses between 0.005 and 0.9 foot, the foils provide even lower absorption rates than the ten shadow shields. For a given value of the abscissa parameter the foil curve is independent of tank diameter, whereas the shadow-shield curves would move upward for diameters greater than 10 feet and move downward for diameters less than 10 feet. A weight comparison between the foils and shadow shields would again be difficult, because the weight optimization would involve the thermal-protection system, the structural-weight penalty of this system, and the propellant boiloff.

631545—62——3

THERMAL PROTECTION AGAINST PLANETARY HEATING

Shadow shields.—Figure 10 shows a cylindrical cryogenic tank at low altitude above a planet surface, with the longitudinal axis of the tank alined along the Sun-planet line. Radiation from the planet received by the tank end and side surfaces occupies a large solid angle. That is, the angle factors for planetary radiation are large at low altitudes. To intercept even the planetary radiation reaching the tank end with a single shadow shield or several shadow shields would require prohibitively large shields, as shown in the figure, unless the shields are placed very close to the end of the tank. In order to shadow a locally

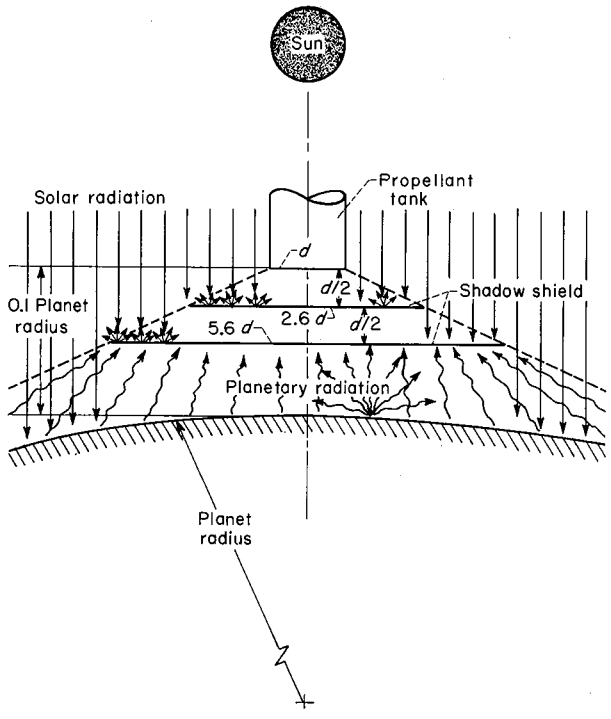

FIGURE 10.—Effects of planetary and solar flux on planetary shadow shields.

horizontal tank surface completely from planetary radiation, the shadow shields must occupy the same solid angle as the planet. The solid angle occupied by a planet increases as the distance from the planet decreases and approaches 2π steradians at the planet surface. Thus, the size of the shadow shield would become prohibitive at low altitudes. Small-diameter shadow shields would provide essentially no protection for the sides of the cryogenic tank. The Sun side of large-diameter planetary shadow shields would be a good reflector of solar radiation. In fact, the effect of reflected solar flux incident on the tank end and side surfaces might even be larger than direct planetary flux on these tank surfaces.

The effectiveness of a simple system of double shadow shields (with diam. equal to the propellant-tank diam.) in reducing the hydrogen heat-absorption rate of the tank end due to planetary radiation is shown in figure 11. Again, the stage is assumed to be oriented with its longitudinal axis alined along the Sun-Earth line. In this position solar flux is not directly incident upon either the tank sides or the tank end facing the planet. However, solar flux is reflected from the planet surface onto both the tank end and tank sides. For figure 11 the emissivity and absorptivity are assumed equal to 0.1. Figure 11(a) shows the shadow-shield spacing ratio that minimizes the hydrogen heat-absorption rate plotted against the ratio of altitude above Earth's surface to Earth's radius. These spacing ratios decrease rapidly for decreasing abscissa values of less than 1. At a value of (altitude/planet radius) of 0.1, the heat-absorption rate is minimized with the small spacing ratio of about 0.00001 (which corresponds to a spacing between 10-ft-diam. shields of 0.0012 in.). The heat-absorption rates that correspond to these spacing ratios are shown in figure 11(b). For reference, the upper curve shows the absorption rate for two closely spaced foils. As might be expected from the theory, the shadow-shield and foil curves approach each other when the optimum spacing between shadow shields is extremely small (at low altitudes).

In order to compare the magnitude of the heat-absorption problem in the vicinity of planets other than Earth, figure 12 is included. For this figure it was arbitrarily assumed that the spacing ratio l/d between adjacent shadow shields was 0.1 and that emissivity and absorptivity were also equal to 0.1. Heat transfer only on the end of the tank facing the planet was assumed. The hydrogen heat-absorption rate is shown against the ratio of altitude above the planet surface to planet radius for Venus, Earth, and Mars. Venus, Earth, and Mars rank highest to lowest in that order, comparing the heat-absorption rates at a constant value of the ratio of altitude to planet radius. For low altitude ratios, the absorption rates are of the order of 700 to 140 Btu/(day)(sq ft end area), which are prohibitively high for most applications.

Foils.—The effectiveness of foil materials in reducing the hydrogen heat-absorption rate due to planetary heating can be substantial, as shown in figure 13. It was assumed for this figure that the absorption rates are due only to the heat transfer through the surface specified and that the stage is alined on the Sun-Earth axis as in the sketch. Foils are assumed to cover completely the tank sides and tank end facing the Earth. Hydrogen heat-absorption rate is shown against the number of foils for $\alpha=\epsilon=1$, 0.1, and 0.01. Also shown for reference are absorption rates with no foils on the tank. Either increasing the

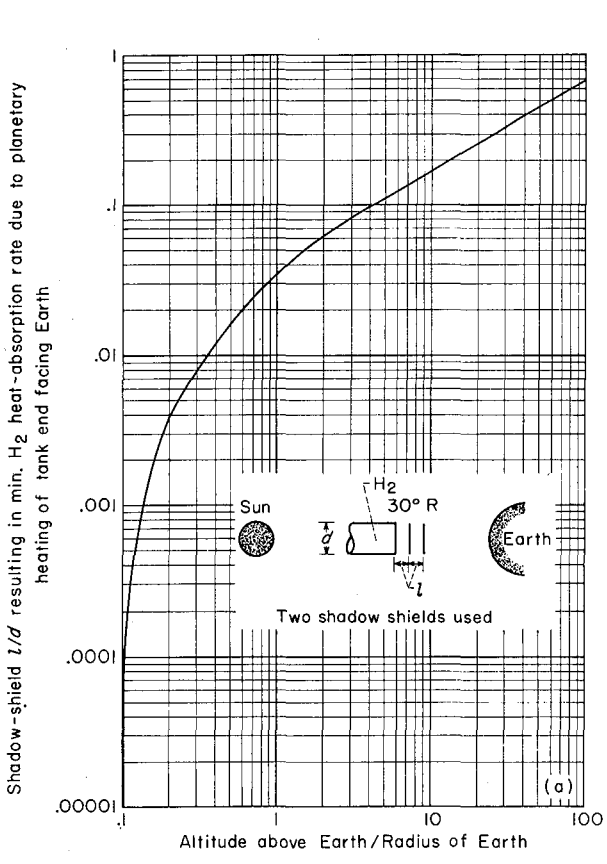

(a) Effect of altitude on optimum spacing of double shadow shields.

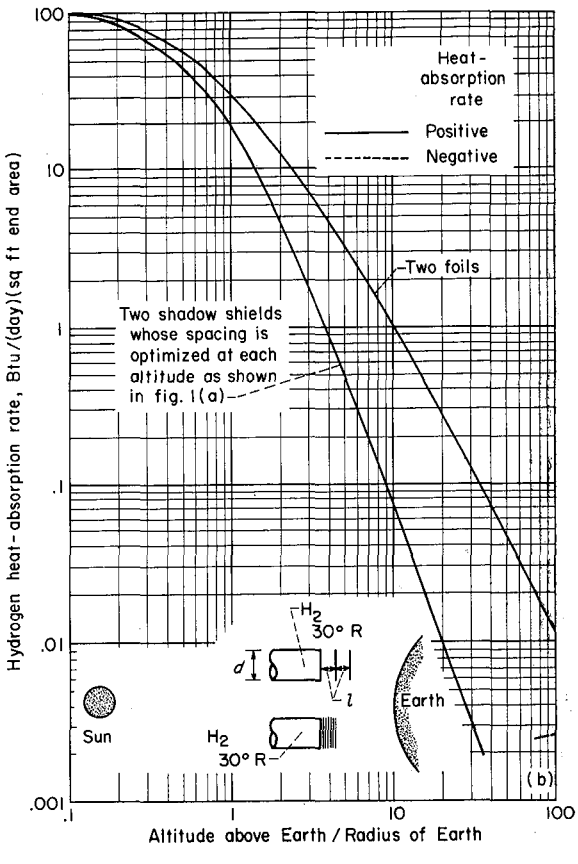

(b) Hydrogen heat-absorption rate corresponding to optimum shadow-shield spacing.

FIGURE 11.—Shadow shields for reducing heating effect of Earth flux on hydrogen-tank end ($\alpha=\epsilon=0.1$).

number of foils or decreasing the foil emissivity decreases the hydrogen heat-absorption rate. Absorption rates on the tank sides are less than those on the tank end, because the vertical angle factor is less than the horizontal angle factor for a particular altitude. However, foils would still be required on the tank sides to achieve low absorption rates.

Combinations of shadow shields and foils.—Figure 14 shows the hydrogen heat-absorption rate against the number of foils (foils immediately adjacent to the tank end) behind a system of two shadow shields for a tank end facing the Earth and located on the Sun-Earth axis at an altitude above the Earth's surface of 0.1 Earth radius. A shadow-shield spacing ratio of 0.1 was used. Emissivity and absorptivity were assumed equal to 1, 0.1, and 0.01. Decreasing emissitivity and increasing the number of foils both decreased the heat-absorption rate. For reference, a curve of absorption rate for a configuration with foils but no shadow shields and with $\alpha=\epsilon=0.1$ is included. Because the altitude is relatively low and the angle factor for the planet is relatively high, this configuration (with no shadow shields) provides heat-absorption rates that are almost as low as the comparable configuration with shadow shields. Also included for reference are horizontal dashed lines for configurations with no foils (i.e., two shadow shields only). From the figure it appears that the benefits derived from widely spaced planetary shadow shields for protection of tank surfaces for low-altitude planet approaches are generally small. By augmenting the shadow shields with foils, lower heat-absorption rates are possible; however, foils alone give practically the same heat-absorption rates.

Trajectory variables.—Thus far, the methods of protecting a cryogenic-tank surface from external heating have included using shadow shields, foils,

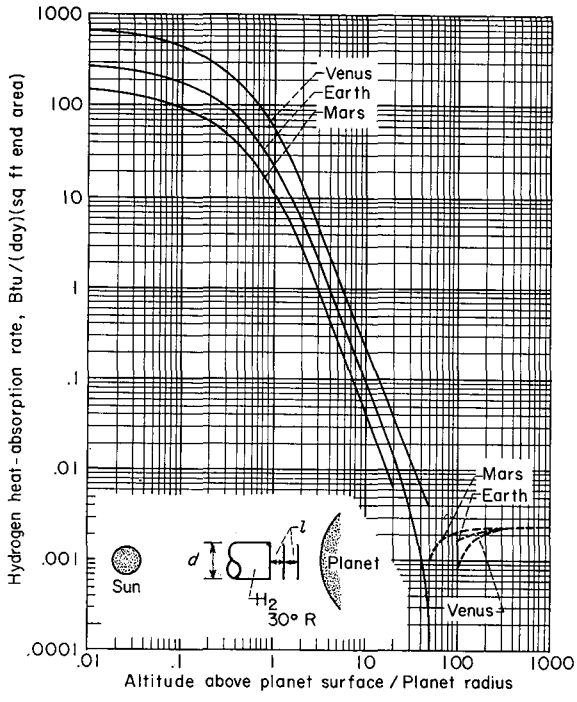

FIGURE 12.—Effect of altitude above several planets on hydrogen heat-absorption rate with double shadow shields ($l/d=0.1$; $\alpha=\epsilon=0.1$).

combinations of these, orientation, and special coating materials. One other factor that should be included here is trajectory considerations, since the total heat absorbed on any mission will be the integral of the heat-absorption rate with respect to time. These trajectory effects are considered in detail in reference 8.

As mentioned previously, the heat-absorption rate due to planetary heating is a strong function of the altitude above the planet. If small heat-absorption rates are desired while orbiting a planet, then the vehicle must operate at high altitudes. One means of having low-altitude capabilities and small heat-absorption rates is to utilize elliptic orbits. Here the high heat-absorption rates are encountered only for short time periods, and thus the total heat absorbed per orbit will be much less than the heat absorbed for a low-altitude circular orbit.

Likewise, the escape and entry trajectories are also important in the overall storage problem. Vehicles with low thrust-to-weight ratios will absorb more heat (upon escaping or entering a planet orbit) than will vehicles with high thrust-to-weight ratios. However, as shown in reference 8, for thrust-to-weight ratios greater than about 0.01, escape and entry heat absorption is generally negligible. Most chemical and nuclear rockets have thrust-to-weight ratios greater than 0.1.

Comparison of methods.—The effectiveness of the various thermal-protection techniques for reducing the rate of absorption of flux is shown in figure 15. The hydrogen heat-absorption rates for the end of a cryogenic tank protected by either shadow shields, or foils, or shadow shields with foils, are plotted against the ratio of altitude above Earth to Earth radius. The absorptivity and emissivity were assumed equal to 0.1. It is apparent that the shadow shields are relatively ineffective at low altitudes; however, at high altitudes where the planet flux is more nearly parallel (and almost insignificant in magnitude), the shadow shields are more effective. Augmentation of these shadow shields with foils lowers the heat-absorption rate by a factor of about 10. However, at high altitudes, practically the same absorption rates can be obtained with

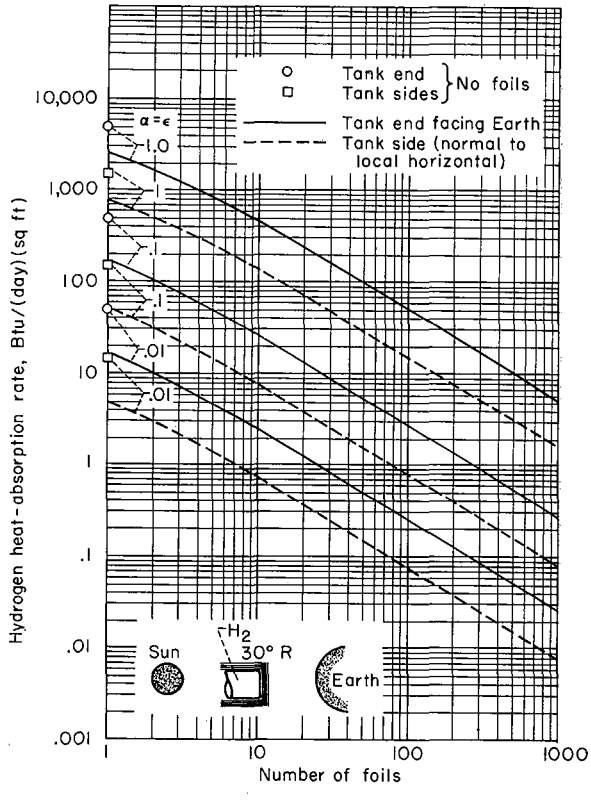

FIGURE 13.—Effect of number and emissivity of foils on hydrogen heat-absorption rate due to planetary flux. Ratio of altitude above Earth to Earth radius, 0.1.

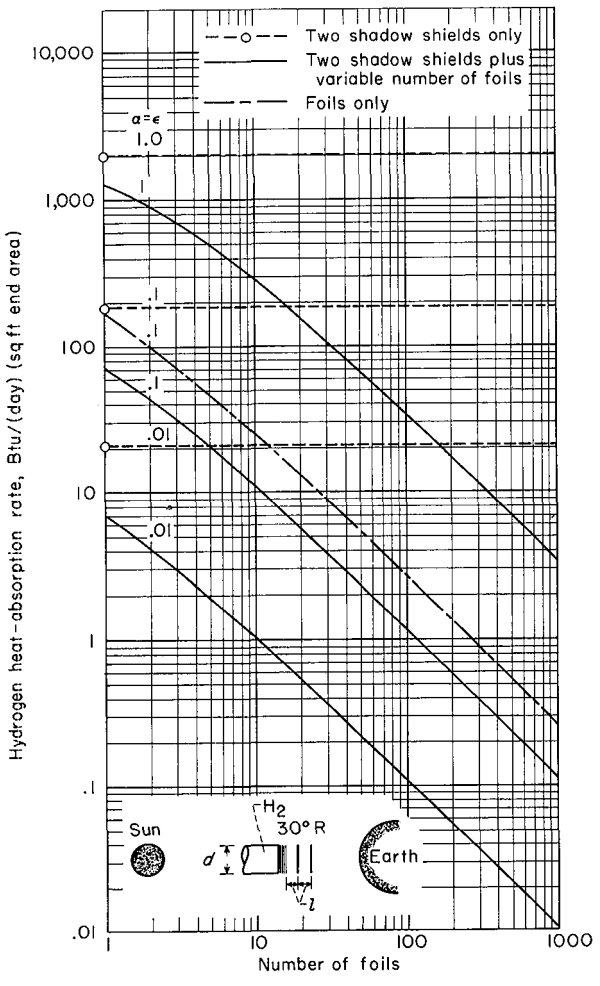

FIGURE 14.—Effect of number of foils and presence of double shadow shields on hydrogen heat-absorption rate due to planetary flux ($l/d=0.1$). Diameter, 10 feet; ratio of altitude above Earth to Earth radius, 0.1.

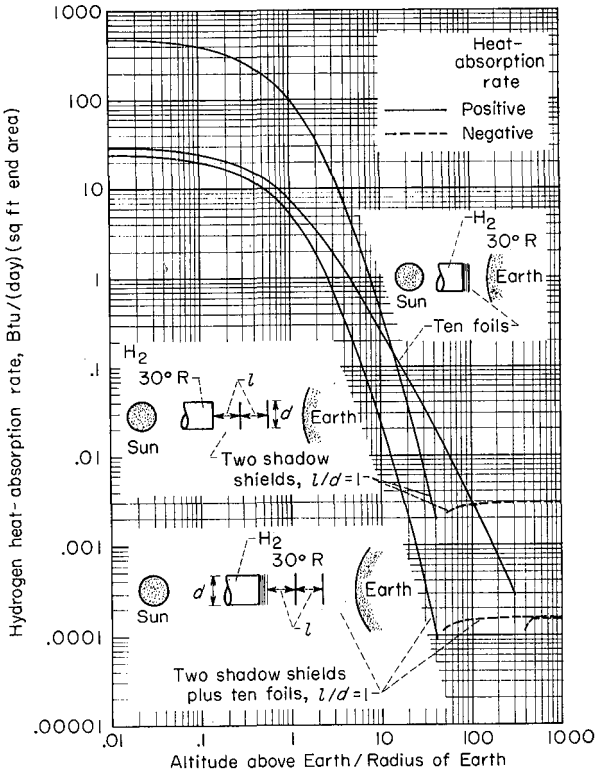

FIGURE 15.—Effectiveness of various devices for reducing effect of planetary heating ($\alpha=\epsilon=0.1$).

foils alone. Thus, it appears that an attractive method of reducing the effect of planetary heating is to employ foils on all surfaces, since the additional advantage of using shadow shields is relatively small. Below altitudes of about 2.2 Earth radii, the ten foils are at least an order of magnitude more effective than two shadow shields. At 14 Earth radii, the two are equivalent. A possible disadvantage of planetary shadow shields is that they will require a continuous orientation toward the planet, thus allowing the cryogenic-tank surfaces to be exposed to direct solar flux.

Any other shadow-shielding system considered herein will lose its efficiency as a planet is approached. For example, an internal shadow-shielding system that is sufficient in space will probably be insufficient near a planet where the external heating can affect it. Again, it should be emphasized that the mission plays a major role in determining the protection system. If only a short time is to be spent near a planet, the shadow-shielding systems will no doubt suffice. However, for long parking times in orbit, widely spaced shadow-shielding systems will have to be either replaced by an alternative shielding system or augmented with foils. The choice of a complete thermal-protection system will ultimately be based on the minimum payload weight penalty.

DESIGN OF A TYPICAL THERMAL-PROTECTION SYSTEM

Thus far, the methods of thermally protecting a cryogenic tank have, in general, been treated by considering an isolated portion of the tank subjected to a constant internal or external flux. The purpose of this section is to integrate these findings and demonstrate a method of minimizing the payload weight penalty of a complete protection system for a particular space vehicle and for specific missions. All cryogenic-tank surfaces

will be considered, and a variety of heating environments will prevail. The vehicle used will be a hydrogen-oxygen terminal stage. A terminal stage has been selected because it usually is exposed to the most severe heating environment.

The stage assumed has the hydrogen and oxygen stored in 10-foot-diameter cylindrical tanks at 30° and 140° R, respectively. The hydrogen and oxygen tanks are 10 and 3.5 feet long, respectively.

Two missions have been selected: (1) a 179-day one-way trip, which uses its terminal stage propellants to place a payload in orbit about Mars, and (2) a 378-day round trip to Mars, which includes 20 days spent in a 1000-statute-mile circular orbit about Mars. For the round trip it is assumed that, after the 20-day waiting period, the terminal-stage propellants are used to put the payload on a coast trajectory for return to Earth.

It is assumed that the stage components are arranged in the following order: payload, oxygen tank, hydrogen tank, and engine. From figures 6 to 9 it was concluded that exposure of a cryogenic-tank surface to direct solar flux was impractical. By orienting the stage with the payload pointed at the Sun, the heating effect of solar flux was avoided.

With the stage oriented so that the payload faces the Sun, the thermal-protection-system design will be based on the effects of other external radiation and the radiation between components.

If it is assumed that the payload weight of the terminal stage is to be maximized, a relation between payload weight, boiloff weight, and thermal-protection weight can be developed. The stage gross weight is

$$W_g=W_{pl}+W_{up}+W_{st}+W_{bo}+W_{tp}$$

where W_{bo} is the propellant vented overboard as a vapor because of heat absorption by the propellant tanks (not a part of W_{up}). If the material used for thermal protection is not jettisoned before the propellants are burned, then

$$W_{up}=\left(1-\frac{1}{e^{\Delta v/Ig}}\right)(W_g-W_{bo})$$

The structure weight can be approximated as follows:

$$W_{st}=W_g\left[0.08\,\frac{(W_{up}+W_{bo})}{W_g}+0.02\,\frac{F}{(W_g-W_{bo})}\right]$$

where $0.08\ (W_{up}+W_{bo})$ and $0.02\ F$ are representative values for the tankage structure weight and the thrust sensitive weight, respectively. The uncertainty of the coefficient 0.02 is such that this expression can be written with equal accuracy as

$$W_{st}=W_g\left[0.08\,\frac{(W_{up}+W_{bo})}{W_g}+0.02\,\frac{F}{W_g}\right]$$

If these expressions for propellant and structural weight are substituted in the original expression for gross weight, the resultant expression is

$$W_g=\frac{W_{pl}+W_{tp}+W_{bo}\left(\frac{1.08}{e^{\Delta v/Ig}}\right)}{\frac{1.08}{e^{\Delta v/Ig}}-0.08-0.02\,\frac{F}{W_g}}$$

or, in a more convenient form,

$$W_{pl}=W_g\left(\frac{1.08}{e^{\Delta v/Ig}}-0.08-0.02\,\frac{F}{W_g}\right)-W_{tp}-W_{bo}\left(\frac{1.08}{e^{\Delta v/Ig}}\right)$$

where F/W_g is the thrust-to-gross-weight ratio. From this final expression for W_{pl}, it is apparent that, for fixed values of W_g, Δv, I, and F/W_g, the payload weight is

$$W_{pl}=\text{const.}-\left[W_{tp}+W_{bo}\left(\frac{1.08}{e^{\Delta v/Ig}}\right)\right]$$

Thus, in order to maximize the payload weight, it will be necessary to minimize the sum of the thermal-protection weight and $1.08/e^{\Delta v/Ig}$ times the boiloff weight. For the Mars trips being considered, a terminal-stage Δv of 3.35 miles per second and a value of 0.5 for F/W_g were assumed. A value of 425 seconds was assumed to be a representative value of specific impulse for this hydrogen-oxygen stage.

Propellant boiloff has been shown in figures 2 to 15 to be strongly dependent on the radiation environment and the thermal-protection devices used. Furthermore, the radiation environment will ordinarily change as the mission progresses. Additional assumptions will be introduced as the one-way and round-trip payload weights are being maximized.

Mars one-way trip.—It was stated previously that the payload was pointed at the Sun. Because

the thrust-to-weight ratio was large (0.5), the effects of Earth and Mars radiation (during the escape trajectory from Earth and during the Mars entry trajectory) were negligible. Thus, the only remaining modes of radiation affecting boiloff were the radiation between components of the vehicle and radiation from the propellants to space. Because hydrogen has a heat of vaporization more than twice that of oxygen, it is desirable to vaporize hydrogen instead of oxygen. This ignores the opposing (but negligible in this case) effect of greater hydrogen tank weight because oxygen is more dense than hydrogen.

Figure 16 shows the effect of variation of the number of intercomponent foils on the payload weight penalty (defined as $W_{tp}+(1.08/e^{\Delta v/Ig})W_{bo}$).

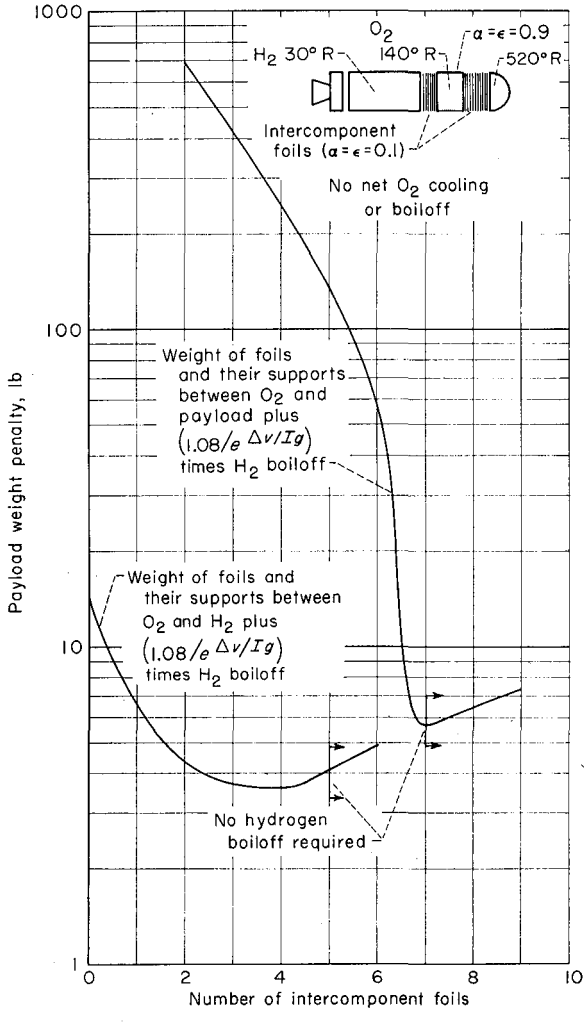

FIGURE 16.—Variation of payload weight penalty with number of foils between components.

It was assumed that all foils have $\alpha=\epsilon=0.1$ (refs. 20 to 22), and that the oxygen-tank side has $\alpha=\epsilon=0.9$. The weights of the stage were as follows: W_g=30,287 pounds (13,738 kg), W_{up}= 21,970 pounds (9965 kg), W_{st}=2060 pounds (934 kg). Because the tank sides received no radiation from the Sun and negligible radiation from the planets and space, it was possible to use the tank sides (and engine end of the hydrogen tank) to reject excess heat to space. The emissivity of these surfaces was chosen as 0.9. For all other surfaces it was desirable to have the lowest acceptable value of emissivity (0.1). Foil weights were based on (1) foil weight of 0.01 pound per square foot of foil (ref. 20), and (2) foil support weight of 0.03 pound per foil based on a 10-foot-diameter area and a foil density of 50 foils per inch. As shown in figure 16, the optimum numbers of foils between the payload and the oxygen tank and between the hydrogen and oxygen tanks were 7 and 4, respectively. The total payload weight penalty for this stage is only about 10 pounds. This is only about 0.16 percent of the 6245-pound (2833 kg) payload weight of the stage.

The payload weight penalty of this stage due to thermal radiation is extremely small. Thus, heat transfer by some other mode (conduction through the structure, e.g.) could easily have a larger effect on payload weight than propellant heating by radiation. With the almost negligible weight penalty due to the small number of foils, it is not necessary to resort to isolated shadow-shield systems as shown in figure 3 to reduce further the rate of heat transfer from the payload to the oxygen tank

Mars round trip.—It was shown previously that the payload weight penalty due to thermal radiation for a 179-day one-way trip to Mars is essentially negligible. Also, figures 10 to 15 show that thermal-radiation effects in the vicinity of a planet can be several orders of magnitude larger than radiation effects in interplanetary space. Thus, for the round trip suggested, which included orbiting Mars for 20 days in a 1000-mile circular orbit, it should be anticipated that the payload weight penalty due to thermal radiation will be much larger than the penalty for the one-way trip.

In optimizing the thermal-protection system for the round trip, the following assumptions were made:

(1) The thermal-protection system had fixed

elements (i.e., no variable-geometry devices were considered).

(2) For all coast phases of the trip, the payload was pointed at the Sun.

(3) To prevent freezing of the propellants, no net heat loss was allowed for either the hydrogen or oxygen for any part of the trip.

(4) If a choice existed, hydrogen boiloff was used instead of oxygen boiloff to conserve weight.

(5) Propellant boiloff was assumed to occur at 1 atmosphere. The magnitude of propellant boiloff was calculated by dividing the heat input by the heat of vaporization at 1 atmosphere.

(6) For all surfaces the emissivity and absorptivity were equal. Values were limited to the range 0.1 to 0.9.

(7) The installed weight of foils was the same as mentioned in the previous example.

(8) The Mars parking orbit was circular at an altitude of 1000 statute miles and contained the Sun-Mars axis.

(9) The stage velocity increment was 3.35 miles per second.

(10) The specific impulse was 425 seconds.

The heat-absorption rates for the end of the hydrogen tank and the sides of the oxygen and hydrogen tanks, all protected by ten foils ($\alpha=\epsilon=$ 0.1), are shown in figure 17 against angular position of the stage with respect to the Sun-Mars axis. Two factors that affect these curves profoundly are the variation of planetary flux with angular position around the planet and the variation of angle factors with angular position. The planetary flux varies with the temperature of the planet and also with the planet's albedo. Because the planet's temperature and albedo are not precisely known for various positions around the planet (and probably vary from day to day at a fixed position, anyway), the planetary flux cannot be predicted with great precision. Two positions where the flux and consequently the absorption rate may be easily estimated are the 0° (full daylight) and 180° (midnight) positions. For figure 17, the 90° and 270° values were obtained by taking the arithmetic mean value between those computed assuming a fully sunlit planet and a fully darkened planet. The flux between these points was assumed to vary according to a sine relation, the result of which is shown in figure 17. For simplicity, it was assumed that the angle factors were between either fully sunlit or fully shadowed planet surfaces and either locally horizontal or vertical tank surfaces.

By integrating the curves of figure 17, the average heat-absorption rates for a complete orbit are obtained. However, there is no reason to believe that the arbitrarily assumed number of foils (10) is also the optimum number of foils. This presents no particular difficulty in the optimization process, because (from eq. (14) in the ANALYSIS) it can be seen that, if it is assumed that $\alpha_S=\epsilon_o=\epsilon_x=\epsilon_y$, then the absorption rate on these external surfaces must be proportional to $\epsilon/[N(2-\epsilon)+1]$.

By using the preceding assumptions, it was possible to minimize the payload weight penalty. The results of this optimization process are shown in the following sketch of the terminal stage:

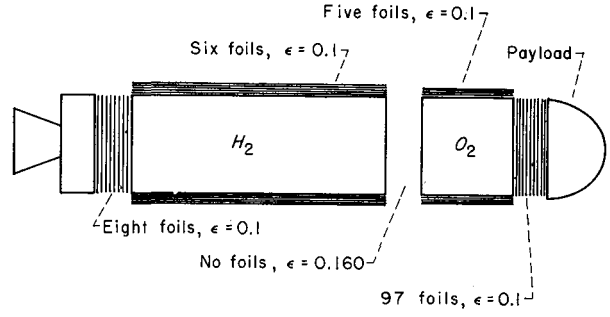

(e)

The number and emissivity of the foil surfaces are indicated. A higher value of emissivity between the oxygen and hydrogen tanks would have resulted in freezing of the oxygen during the 179-day coast from Earth to Mars. The foils and their supports weigh 110 pounds (50 kg). During the 179-day phase of the trip, 99 pounds of hydrogen and no oxygen are vaporized and vented. During the 20 days in the Mars orbit, 100 pounds of hydrogen and 57 pounds of oxygen are vaporized and vented. The total propellant boiloff is therefore 256 pounds (116 kg). Thus, the payload weight penalty

$$\frac{100\%}{W_{pl}}\left[W_{tp}+\left(\frac{1.08}{e^{\Delta v/Ig}}\right)W_{bo}\right]$$

is only about 3 percent. Other weights are as follows: net payload, 6108 pounds (2770 kg); gross, 30,526 pounds (13,841 kg); structure, 2083 pounds (945 kg); and propellants, 21,970 pounds (9965 kg).

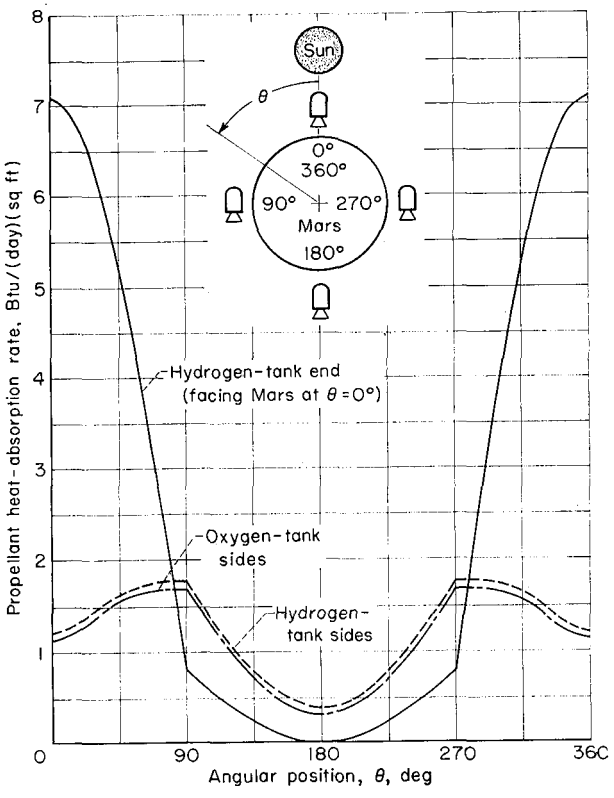

FIGURE 17.—Variation of heat-absorption rate with angular position for stage in circular orbit 1000 statute miles above Mars surface. Ten foils on hydrogen- and oxygen-tank sides and on hydrogen-tank end ($\alpha=\epsilon=0.1$).

Solar alinement.—For both the one-way and round trips, it was assumed that the payload was perfectly alined with the Sun. With other than perfect alinement of the vehicle axis, direct solar flux would be incident upon the cryogenic-tank sides. This would produce propellant losses and degradation of the velocity-increment potential of the stage. A detailed treatment of the effect of tank alinement with respect to the Sun on boiloff losses is presented in reference 5. The magnitude of these boiloff losses is shown in figure 18 for both the one-way and round-trip configurations. Integrated boiloff losses are shown for the 179-day phase of the trips against the angle of misalinement with respect to the Sun. For misalinement angles greater than about 2.2°, both the hydrogen and oxygen losses exceed 100 pounds using the round-trip stage. Because the one-way-trip stage has no foils on the tank sides and instead uses highly absorptive surfaces, its losses are about 100 times greater than for the round-trip stage. As

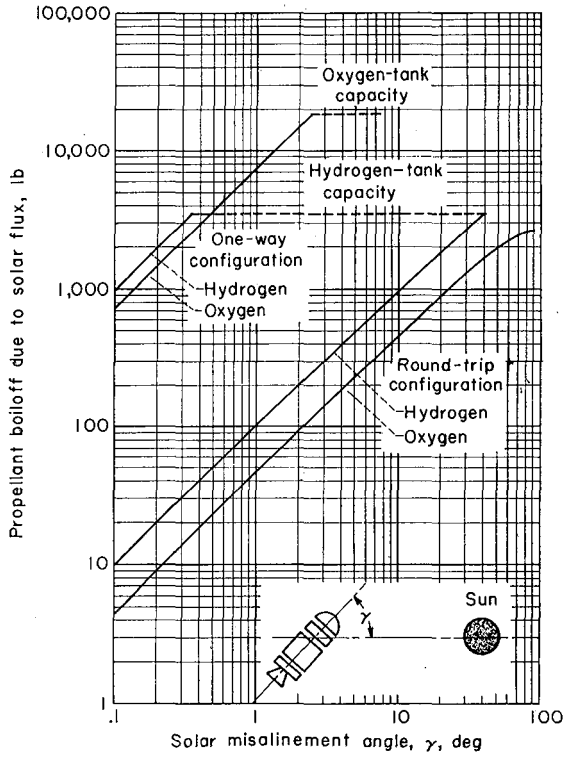

FIGURE 18.—Effect of stage misalinement angle with respect to local solar flux on propellant loss for one-way and round-trip configurations.

shown previously, these losses are proportional to $\epsilon/[\bar{N}(2-\epsilon)+1]$.

It would be possible to include the effect of solar misalinement in the payload weight optimization. An obvious passive method of eliminating propellant boiloff due to solar misalinement is to construct the stage in the form of a cone (instead of cylinder), as shown in sketch (f). Solar misalinement angles as large as $\beta/2$ could be tolerated with no propellant loss due to solar flux.

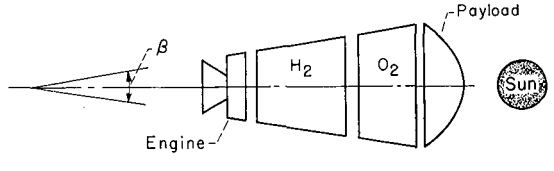

(f)

CONCLUDING REMARKS

The analytical techniques developed in this report provide the basic information required to design thermal-protection systems for propellant tanks subjected to the thermal-radiation environ-

ment of space. The application of these theoretical relations has been demonstrated for cryogenic-propellant tanks. However, the methods used herein are equally applicable whether cryogenic or noncryogenic propellants are considered.

Thermal-protection systems have been discussed in detail. The optimum method of providing thermal protection for cryogenic propellants is strongly dependent upon the magnitude and duration of the thermal environment encountered during the mission.

Shadow shields and foils can greatly reduce the heating of propellants due to both internal and external thermal radiation. For low-altitude planetary orbits, foils appear to be desirable for all cryogenic-tank surfaces exposed to planetary or solar radiation.

The proper orientation of a space-vehicle cryogenic tank with respect to the Sun is one of the most beneficial methods of reducing the heating effect of solar flux.

It is recognized that several other factors, such as aerodynamic heating during the boost trajectory, weightless fluid-dynamic phenomena, meteoroid penetrations (ref. 23), effect of meteoroids on reflective surfaces (ref. 24), materials problems (ref. 25), and nuclear-radiation heating, may have an important effect on the choice of a thermal-protection system.

LEWIS RESEARCH CENTER
NATIONAL AERONAUTICS AND SPACE ADMINISTRATION
CLEVELAND, OHIO, *August 3, 1961*

APPENDIX A

SYMBOLS

A	cross-sectional area, sq ft
a	albedo=1−emissivity=reflectivity
d	diameter, ft
F	thrust
f	angle factor
g	acceleration due to gravity at Earth's surface, ft/sec^2
h	altitude, statute miles
I	specific impulse, sec
k	apparent mean thermal conductivity of insulation, (Btu)(in.)/(sq ft)(hr)(°R)
l	distance between radiation shields, ft
N	number of radiation shields
$\dot{Q}$	heat-transfer rate, Btu/hr
r	radius, ft
T	temperature, °R
t	thickness of insulation, in.
Δv	stage velocity increment, ft/sec
W	weight, lb
x,y	any surfaces or tank surfaces
Y	external heat flux, incident upon bare tank or tank protection system, Btu/(sq ft)(hr)
z	$z=1$ on Sun side of planet; $z=0$ on dark side of planet
α	total hemispherical absorptivity
α_S	total hemispherical absorptivity of a surface for solar radiation
δ	see eq. (2)
ϵ	total hemispherical emissivity
ϵ_o	total hemispherical emissivity of outermost surface at surface temperature
ρ	radius, statute miles
σ	Stefan-Boltzmann constant, 1.713×10^{-9} Btu/(sq ft)(hr)(°R^4)

Subscripts:

a	circular portion of shield shaded by adjacent tank or shield
B	all surfaces facing inward to propellant tank
b	annular portion of shield not shaded by adjacent tank or shield
bo	boiloff
F	all surfaces facing outward from propellant tank
g	gross
max	maximum
n	net
o	reflective surface upon which external radiation is incident
P	relative to planet, or planet
pl	payload
S	Sun or solar
S,P	Sun to planet
s	relative to space, or space
st	structure
tot	total
tp	thermal protection
up	useful propellant
v	vertical
x	adjacent tank
y	tank for which heat-absorption calculations are being made

APPENDIX B

ANGLE FACTORS

The angle factor $f_{1,2}$ is defined as the fraction of radiant energy leaving surface dA_1 that is directly intercepted by surface A_2. Assuming diffuse radiation and the cosine law of Lambert, $A_1 f_{1,2}$ is

$$A_1 f_{1,2} = \int_{A_1} \int_{A_2} \left(\frac{\cos \varphi_1 \cos \varphi_2}{\pi r^2} \right) dA_1 \, dA_2 = A_2 f_{2,1}$$

where the geometry is defined by sketch (g). This relation was derived in reference 26. The angle factors presented herein are based on the preceding assumptions.

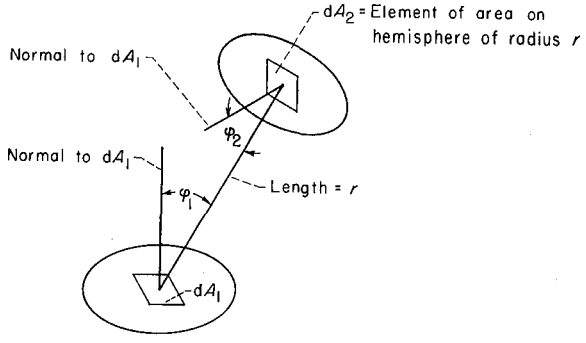

(g)

DIRECTLY OPPOSED PARALLEL DISKS

The angle factor for directly opposed parallel disks (based on ref. 27) (sketch (h)) is

$$f_{1,2} = \frac{1}{2}\left[1 + \left(\frac{r_2^2 + l^2}{r_1^2} \right) - \sqrt{\left(1 + \frac{r_2^2 + l^2}{r_1^2} \right)^2 - 4\left(\frac{r_2^2}{r_1^2} \right)} \right] \quad \text{(B1)}$$

where

$$A_1 = \pi r_1^2$$

$$A_2 = \pi r_2^2$$

and

$$f_{1,2} A_1 = f_{2,1} A_2$$

If $r_1 = r_2$, equation (B1) becomes identical to an independently derived angle factor for the same example (eq. (A5)) in reference 18.

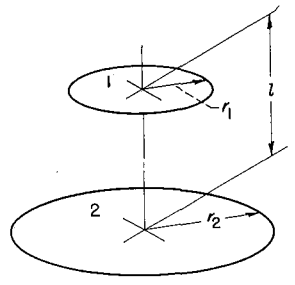

(h)

DIRECTLY OPPOSED PARALLEL ANNULI

The angle factor for directly opposed parallel annuli (also based on ref. 27) (sketch (i)) is

$$f_{1,4} = \frac{1}{2}\left[\left(\frac{r_4^2 - r_3^2}{r_1^2} \right) - \sqrt{\left(1 + \frac{r_4^2 + l^2}{r_1^2} \right)^2 - 4\left(\frac{r_4^2}{r_1^2} \right)} + \sqrt{\left(1 + \frac{r_3^2 + l^2}{r_1^2} \right)^2 - 4\left(\frac{r_3^2}{r_1^2} \right)} \right] \quad \text{(B2a)}$$

$$f_{2,4} = \frac{1}{2(r_2^2 - r_1^2)} \left[\sqrt{(r_2^2 + r_3^2 + l^2)^2 - (2r_3 r_2)^2} - \sqrt{(r_2^2 + r_4^2 + l^2)^2 - (2r_2 r_4)^2} + \sqrt{(r_1^2 + r_4^2 + l^2)^2 - (2r_1 r_4)^2} - \sqrt{(r_1^2 + r_3^2 + l^2)^2 - (2r_1 r_3)^2} \right] \quad \text{(B2b)}$$

where

$$A_1 = \pi r_1^2$$

$$A_2 = \pi (r_2^2 - r_1^2)$$

$$A_3 = \pi r_3^2$$

$$A_4 = \pi (r_4^2 - r_3^2)$$

$$f_{1,4} A_1 = f_{4,1} A_4$$

$$f_{2,4} A_2 = f_{4,2} A_4$$

and r_3 may be zero.

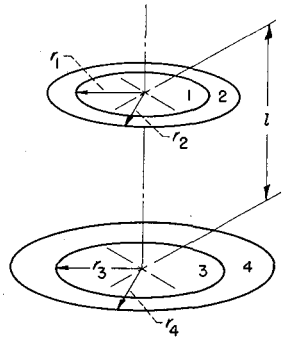

(i)

HORIZONTAL SURFACE AND SPHERICAL PLANET

The angle factor between a locally horizontal surface and either a spherical planet or a flat plate subtending the same apparent solid angle as a planet (sketch (j)) is

$$f_{1,2}=\left(\frac{1}{1+\frac{h}{\rho_P}}\right)^2=f_{F1,P} \tag{B3}$$

This relation and the one that follows are presented in reference 3. In reference 28 they are verified and presented in a more general manner.

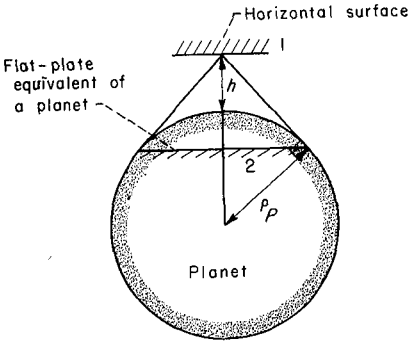

(j)

VERTICAL SURFACE AND SPHERICAL PLANET

The angle factor between a locally vertical surface and either a spherical planet or a flat plate subtending the same apparent solid angle as a planet (sketch (k)) is

$$f_{1,2}=\frac{1}{\pi}\left[\tan^{-1}\left(\frac{\rho_P/h}{\sqrt{1+\frac{2\rho_P}{h}}}\right)-\frac{\left(\frac{\rho_P}{h}\right)\sqrt{1+\frac{2\rho_P}{h}}}{\left(1+\frac{\rho_P}{h}\right)^2}\right]=f_v \tag{B4}$$

MULTIPLE HORIZONTAL SURFACES AND PLANET

The angle factor between a circular, flat, locally horizontal shield and a planet when separated by another shield is shown in sketch (*l*). It has been assumed that the diameters of both horizontal surfaces are equal ($d_1=d_2$) and that the centers of the circular shields are on a planet radius. As previously, the flat-plate equivalent of the planet is assumed.

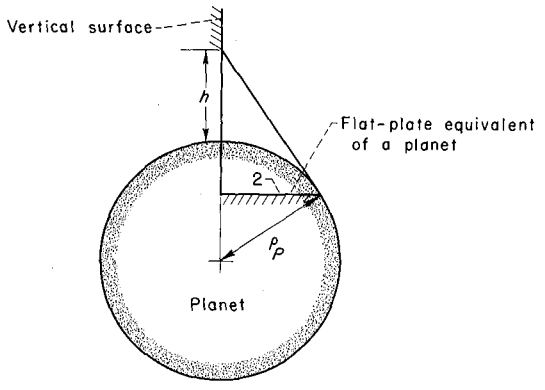

(k)

The angle factor between shield 2 and a planet is defined as

$$f_{F2,P}\equiv f_{F1,P}\frac{(f_{2b,1P}-f_{2b,1})}{f_{2b,1P}}\equiv f_{2b,P} \tag{B5}$$

where $f_{F1,P}$ is the angle factor between a horizontal plate and a planet (given previously in this appendix); $f_{2b,1}$ is the angle factor between the annular area b on shield 2 and shield 1, which can also be calculated with the equations previously given in this appendix; and $f_{2b,1P}$ is the angle factor between the annular area b on shield 2 and the projected area of the planet on surface 1.

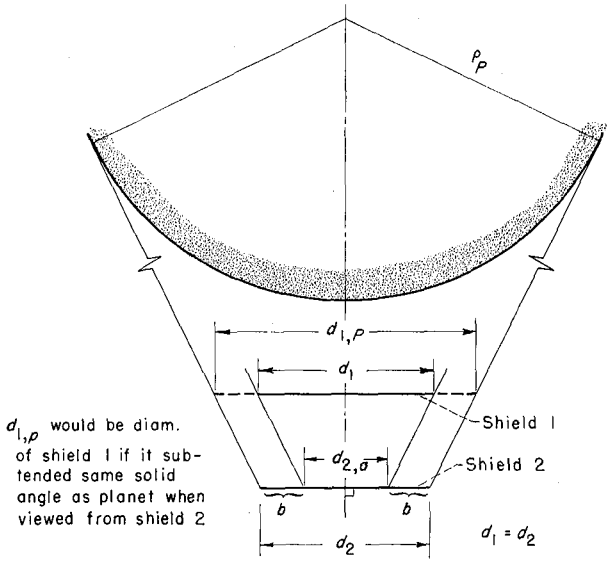

(*l*)

APPENDIX C

GENERAL METHOD OF CALCULATING THERMAL RADIATION BETWEEN ADJACENT SURFACES

The general model used to calculate the exchange of thermal radiation between adjacent reflective surfaces (assuming radiation equilibrium, uniform temperatures, and emissivities and absorptivities independent of temperature) is as shown in sketch (m).

This sketch demonstrates the exchange of radiation between two surfaces. The radiant heat emitted by surface x, in the direction of y only, is considered for simplicity. Radiative heat emitted from surface y in the direction of x would follow the same pattern of absorptions and reflections. Diffuse radiation and the cosine law of Lambert were assumed to apply.

Tracing the radiation exchange between these two surfaces shows that (1) radiant heat is emitted from surface x because of its temperature, (2) a portion of the radiant heat that leaves surface x is absorbed by surface y, (3) a portion of this radiant heat that reaches surface y is reflected, (4) a portion of this reflected radiant heat is absorbed by surface x, and (5) a portion is reflected. This series of absorptions and reflections continues on and on.

The total amount of radiant heat that eventually reaches surface y (because of radiation originating from surface x) is

$$\dot{Q}=\sigma\epsilon_x A_x T_x^4 f_{x,y}\alpha_y[1+f_{x,y}f_{y,x}(1-\alpha_x)(1-\alpha_y) + f_{x,y}^2 f_{y,x}^2(1-\alpha_x)^2(1-\alpha_y)^2 + \ldots + f_{x,y}^n f_{y,x}^n(1-\alpha_x)^n(1-\alpha_y)^n]$$

For $0\leq n<\infty$,

$$\dot{Q}=\sigma\epsilon_x A_x T_x^4 f_{x,y}\alpha_y \sum_{n=0}^{\infty}[f_{x,y}f_{y,x}(1-\alpha_x)(1-\alpha_y)]^n$$

But the angle factors must be ≤ 1, and absorptivities must be ≤ 1; therefore, $f_{x,y}f_{y,x}(1-\alpha_x)(1-\alpha_y) < 1$, and the infinite series converges. Thus,

$$\dot{Q}=\frac{\sigma\epsilon_x A_x T_x^4 f_{x,y}\alpha_y}{1-f_{x,y}f_{y,x}(1-\alpha_x)(1-\alpha_y)}$$

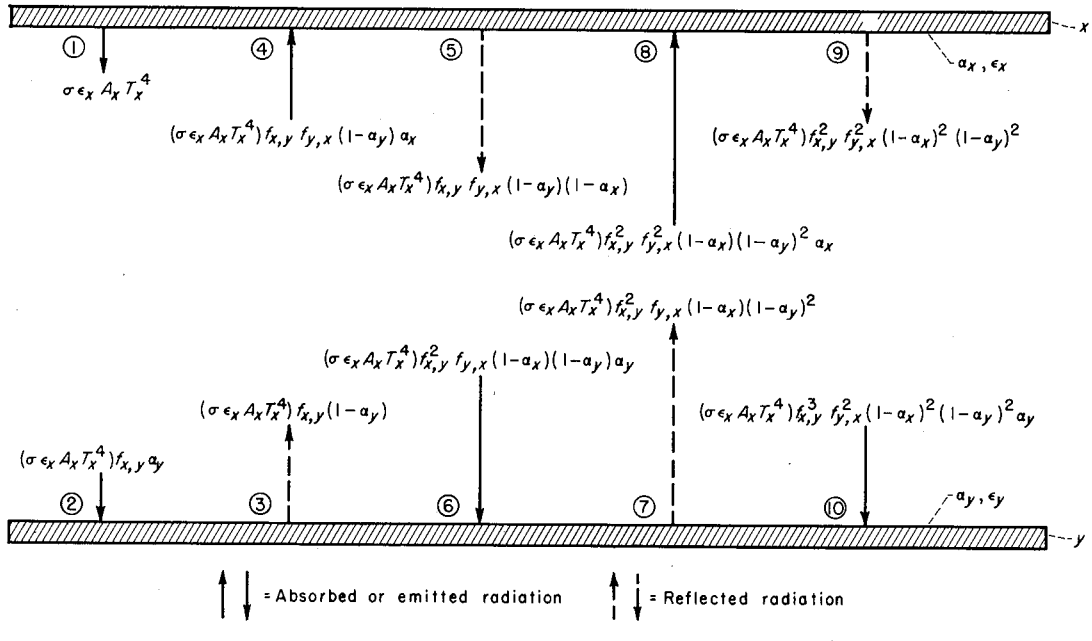

(m)

Similarly, the total amount of radiant heat that eventually returns to surface x because of the many reflections of radiation originating from surface x is

$$\dot{Q}=\sigma\epsilon_x A_x T_x^4 f_{x,y} f_{y,x}(1-\alpha_y)\alpha_x \sum_{n=0}^{\infty} [f_{x,y} f_{y,x}(1-\alpha_x)(1-\alpha_y)]^n$$

$$\dot{Q}=\frac{\sigma\epsilon_x A_x T_x^4 f_{x,y} f_{y,x}(1-\alpha_y)\alpha_x}{1-f_{x,y} f_{y,x}(1-\alpha_x)(1-\alpha_y)}$$

By using the methods developed, the general heat-transfer model in sketch (n) can be utilized in describing the radiant heat exchange between two constant-temperature sources.

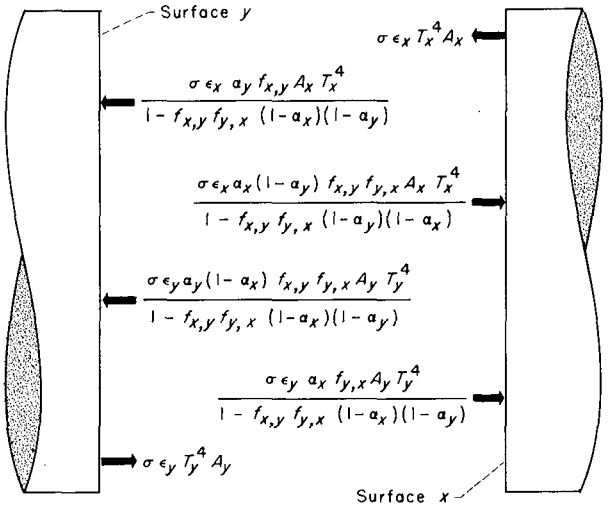

(n)

The terms used here are heat-transfer rates and are components of the overall radiant heat exchange. From the preceding, it is apparent that the net rate of heat emission from surface x (assuming the environmental temperature is 0° R and $A_x=A_y$) is

$$\left(\frac{\dot{Q}}{A}\right)_{\substack{\text{net emitted}\\ \text{by } x}}=\sigma\epsilon_x T_x^4-\frac{\sigma\epsilon_x\alpha_x(1-\alpha_y) f_{x,y} f_{y,x} T_x^4}{1-f_{x,y} f_{y,x}(1-\alpha_x)(1-\alpha_y)}-\frac{\sigma\epsilon_y\alpha_x f_{y,x} T_y^4}{1-f_{x,y} f_{y,x}(1-\alpha_x)(1-\alpha_y)} \quad \text{(C1)}$$

The resulting net heat-emission rate from such an equation may be positive or negative in sign depending upon the temperatures used. The positive sign will indicate the net rate of heat emission, and the negative sign will indicate the net rate of heat absorption.

Similarly, the net rate of heat absorption by surface y is

$$\left(\frac{\dot{Q}}{A}\right)_{\substack{\text{net absorbed}\\ \text{by } y}}=\frac{\sigma\epsilon_x\alpha_y f_{x,y} T_x^4}{1-f_{x,y} f_{y,x}(1-\alpha_x)(1-\alpha_y)}+\frac{\sigma\epsilon_y\alpha_y(1-\alpha_x) f_{x,y} f_{y,x} T_y^4}{1-f_{x,y} f_{y,x}(1-\alpha_x)(1-\alpha_y)}-\sigma\epsilon_y T_y^4 \quad \text{(C2)}$$

If the resultant net heat-absorption rate is negative in sign, this will indicate that this particular surface has a net rate of heat emission rather than a net rate of heat absorption.

APPENDIX D

THERMAL-PROTECTION METHODS[3]

ON-BOARD PROTECTION

Shadow shields.—If one radiation shield is placed directly between the two equal-diameter constant-temperature sources x and y (sketch (o)), the expression for the net rate of heat absorption by surface y is given by

$$\left(\frac{\dot{Q}}{A}\right)_1=\underbrace{\frac{G^2T_x^4+BGT_y^4}{[\sigma(\epsilon_y+\epsilon_x)-E-H]}}_{D_1}+(H-\sigma\epsilon_y)T_y^4 \quad \text{(D1)}$$

where

$$B=\frac{\sigma\epsilon_y f\alpha_x}{1-f^2(1-\alpha_y)(1-\alpha_x)}$$

$$E=\frac{\sigma\epsilon_x f^2(1-\alpha_y)\alpha_x}{1-f^2(1-\alpha_y)(1-\alpha_x)}$$

$$G=\frac{\sigma\epsilon_x f\alpha_y}{1-f^2(1-\alpha_y)(1-\alpha_x)}$$

and

$$H=\frac{\sigma\epsilon_y f^2(1-\alpha_x)\alpha_y}{1-f^2(1-\alpha_y)(1-\alpha_x)}$$

The angle factor f is the same throughout, because the equal-diameter components and shields are equal distances from each other. Equation (D1) is for the rate of heat transfer between the ends of the components only (i.e., no heat transfer through the sides of the components). Here it is assumed that the temperature of the environment is 0° R and that there is no temperature gradient either in the plane of the shield or normal to the shield.

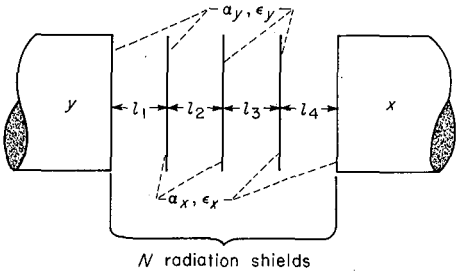

(o)

Using the same assumptions, the net rate of heat absorption by surface y, through a system of two equally spaced radiation shields, is

$$\left(\frac{\dot{Q}}{A}\right)_2=\underbrace{\frac{G^3T_x^4+[\sigma(\epsilon_y+\epsilon_x)-E-H]BGT_y^4}{\{[\sigma(\epsilon_y+\epsilon_x)-E-H]^2-BG\}}}_{D_2}+(H-\sigma\epsilon_y)T_y^4$$

For three shields,

$$\left(\frac{\dot{Q}}{A}\right)_3=\underbrace{\frac{G^4T_x^4+\{[\sigma(\epsilon_y+\epsilon_x)-E-H]^2-BG\}BGT_y^4}{([\sigma(\epsilon_y+\epsilon_x)-E-H]\{[\sigma(\epsilon_y+\epsilon_x)-E-H]^2-BG\}-[\sigma(\epsilon_y+\epsilon_x)-E-H]BG)}}_{D_3}+(H-\sigma\epsilon_y)T_y^4$$

For $N>2$,

$$\left(\frac{\dot{Q}}{A}\right)_N=\frac{G^{N+1}T_x^4+(D_{N-1})BGT_y^4}{[\sigma(\epsilon_y+\epsilon_x)-E-H](D_{N-1})-(D_{N-2})BG}+(H-\sigma\epsilon_y)T_y^4 \quad \text{(D2)}$$

where N is the number of shields, and D_{N-1} and D_{N-2} are the denominators of the fractions in the equations for $N-1$ and $N-2$ shields, respectively.

A further generalization of shadow shields can be made by letting the two constant-temperature bodies have varying diameters as shown in sketch (p). In order to obtain a reasonable solution for this system of shields, it is assumed that the angle factors $f_{y,1}$, $f_{1,2}$, $f_{2,3}$, . . ., $f_{N-1,N}$, and $f_{N,x}$ are all equal. This assumption also dictates that $f_{1,y}, f_{2,1}$, . . ., $f_{N,N-1}$, and $f_{x,N}$ will be equal.

[3] Thermal equilibrium conditions are assumed throughout this appendix.

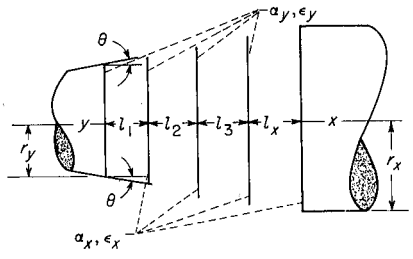

(p)

By examining equation (B1), it is apparent that the angle factors will be equal if

$$\frac{r_1^2+l_1^2}{r_y^2}=\frac{r_2^2+l_2^2}{r_1^2}=\cdots=\frac{r_N^2+l_N^2}{r_{N-1}^2}=\frac{r_x^2+l_x^2}{r_N^2}$$

and if

$$\left(\frac{r_1}{r_y}\right)^2=\left(\frac{r_2}{r_1}\right)^2=\cdots=\left(\frac{r_N}{r_{N-1}}\right)^2=\left(\frac{r_x}{r_N}\right)^2$$

Therefore, r_1/r_y, r_2/r_1, . . ., r_N/r_{N-1}, and r_x/r_N must be equal; and l_1/r_y, l_2/r_1, . . ., l_N/r_{N-1}, and l_x/r_N must be equal. With these relations and the geometry of the system, the radius of any shield and the proper spacing between shields can be obtained from the following equations:

$$r_N=r_y\left(1+\frac{l_1}{r_y}\tan\theta\right)^N$$

$$r_x=r_y\left(1+\frac{l_1}{r_y}\tan\theta\right)^{N+1}$$

$$l_N=l_1\left(1+\frac{l_1}{r_y}\tan\theta\right)^{N-1}$$

and

$$l_x=l_1\left(1+\frac{l_1}{r_y}\tan\theta\right)^N$$

The total length l_{tot} of a shadow-shield system with N shields (neglecting the thickness of the shields) is the sum of all the individual spacings $\sum_{i=1}^{i=N} l_i+l_x$. This can be expressed as

$$l_{tot}=-\frac{r_y}{\tan\theta}\left[1-\left(1+\frac{l_1}{r_y}\tan\theta\right)^{N+1}\right]$$

When $\theta\to 0$, $l_{tot}\to l_1(N+1)$.

If one shield is spaced between the two constant-temperature sources x and y in such a manner that $f_{y,1}=f_{1,x}$, then the net rate of heat absorption by surface y is given by

$$\left(\frac{\dot{Q}}{A_y}\right)_1=\underbrace{\frac{G^2\frac{A_x}{A_y}T_x^4+BGT_y^4}{[\sigma(\epsilon_y+\epsilon_x)-E-H]}}_{D_1}+(H-\sigma\epsilon_y)T_y^4$$

where

$$B=\frac{\sigma\epsilon_y f_{y,1}\alpha_x}{1-f_{y,1}f_{1,y}(1-\alpha_x)(1-\alpha_y)}$$

$$E=\frac{\sigma\epsilon_x f_{1,y}f_{y,1}(1-\alpha_y)\alpha_x}{1-f_{y,1}f_{1,y}(1-\alpha_x)(1-\alpha_y)}$$

$$G=\frac{\sigma\epsilon_x f_{1,y}\alpha_y}{[1-f_{1,y}f_{y,1}(1-\alpha_x)(1-\alpha_y)]}$$

$$H=\frac{\sigma\epsilon_y f_{1,y}f_{y,1}(1-\alpha_x)\alpha_y}{1-f_{1,y}f_{y,1}(1-\alpha_x)(1-\alpha_y)}$$

and A_x and A_y are the areas of surfaces x and y, respectively.

The net rate of heat absorption by surface y with two shadow shields between it and surface x is

$$\left(\frac{\dot{Q}}{A_y}\right)_2=\underbrace{\frac{G^3\left(\frac{A_x}{A_y}\right)T_x^4+[\sigma(\epsilon_y+\epsilon_x)-E-H]BGT_y^4}{\{[\sigma(\epsilon_y+\epsilon_x)-E-H]^2-BG\}}}_{D_2}+(H-\sigma\epsilon_y)T_y^4$$

Where $N>2$,

$$\left(\frac{\dot{Q}}{A_y}\right)_N=\frac{G^{N+1}\left(\frac{A_x}{A_y}\right)T_x^4+(D_{N-1})BGT_y^4}{[\sigma(\epsilon_y+\epsilon_x)-E-H](D_{N-1})-BG(D_{N-2})}+(H-\sigma\epsilon_y)T_y^4$$

where D_{N-1} and D_{N-2} are the denominators of the fractions in the equations for $N-1$ and $N-2$ shields, respectively.

Foils.—Foils are very closely spaced radiation shields, where the angle factor f between adjacent shields is assumed to be equal to 1. The net rate of heat absorption by surface y (when separated from surface x by N foils) can be obtained by setting the angle factor f equal to 1 in the previous equations. Equation (D2) then becomes

$$\left(\frac{\dot{Q}}{A}\right)_N=\frac{\sigma\epsilon_y\left[\left(\frac{\alpha}{\epsilon}\right)_y\left(\frac{\epsilon}{\alpha}\right)_x\right]^{N+1}T_x^4-\sigma\epsilon_y T_y^4}{\left(1-\alpha_y+\frac{\alpha_y}{\alpha_x}\right)\left\{\frac{1-\left[\left(\frac{\alpha}{\epsilon}\right)_y\left(\frac{\epsilon}{\alpha}\right)_x\right]^{N+1}}{1-\left(\frac{\alpha}{\epsilon}\right)_y\left(\frac{\epsilon}{\alpha}\right)_x}\right\}} \quad \text{(D3)}$$

When $(\alpha/\epsilon)_y(\epsilon/\alpha)_x=1$, the expression $\{1-[(\alpha/\epsilon)_y(\epsilon/\alpha)_x]^{N+1}\}/[1-(\alpha/\epsilon)_y(\epsilon/\alpha)_x]$ must be replaced by $(N+1)$.

Insulation.—Two equations can be written for the insulation system shown in sketch (q). The first one defines the net rate of heat absorption

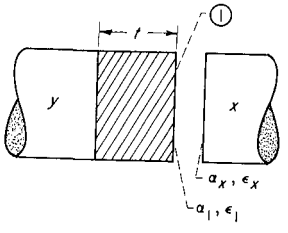

(q)

by surface 1 due to thermal radiation from surface x (see eq. (C2) of appendix C) and is given by

$$\frac{\dot{Q}}{A}=GT_x^4+(H-\sigma\epsilon_1)T_1^4 \qquad \text{(D4a)}$$

where

$$G=\frac{\sigma\epsilon_x f\alpha_1}{1-f^2(1-\alpha_1)(1-\alpha_x)}$$

and

$$H=\frac{\sigma\epsilon_1 f^2(1-\alpha_x)\alpha_1}{1-f^2(1-\alpha_1)(1-\alpha_x)}$$

Equation (D4a) assumes that there is heat transfer only through the ends of the tanks and the insulation and that the surrounding environment is at 0° R.

The other equation that can be written for this system is the expression for the rate of heat absorption by surface y due to conduction through the insulation:

$$\frac{\dot{Q}}{A}=\frac{k}{t}(T_1-T_y) \qquad \text{(D4b)}$$

This equation assumes that there is no heat transfer by radiation through the insulation.

The net rate of heat absorption by surface 1, given by equation (D4a), must be equal to the rate of heat transfer by conduction through the insulation (eq. (D4b)). The unknown temperature T_1 can then be obtained by a trial-and-error process. After T_1 is obtained, the heat-transfer rate can be given by either equation.

Another similar application of insulation is shown in sketch (r). Here again, a trial-and-error solution involving two equations is required. One

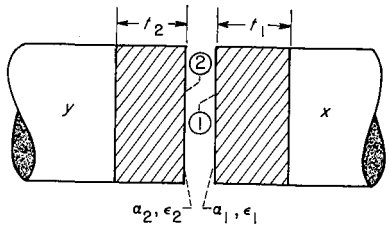

(r)

equation can be obtained by considering the heat-transfer rate through surface 1. The net rate of heat emission by surface 1 must be equal to the heat-transfer rate due to conduction through the insulation t_1. Equating these two heat-transfer rates gives the following:

$$(\sigma\epsilon_1-E)T_1^4-BT_2^4=\frac{k_1}{t_1}(T_x-T_1) \qquad \text{(D5a)}$$

where

$$B=\frac{\sigma\epsilon_2 f\alpha_1}{1-f^2(1-\alpha_1)(1-\alpha_2)}$$

and

$$E=\frac{\sigma\epsilon_1 f^2(1-\alpha_2)\alpha_1}{1-f^2(1-\alpha_1)(1-\alpha_2)}$$

A second equation can be obtained by considering the heat that reaches surface 2. Here, the net rate of heat absorbed by surface 2 must be equal to the heat-transfer rate due to conduction through the insulation t_2. This is given by

$$GT_1^4+(H-\sigma\epsilon_2)T_2^4=\frac{k_2}{t_2}(T_2-T_y) \qquad \text{(D5b)}$$

where

$$G=\frac{\sigma\epsilon_1 f\alpha_2}{1-f^2(1-\alpha_1)(1-\alpha_2)}$$

and

$$H=\frac{\sigma\epsilon_2 f^2(1-\alpha_1)\alpha_2}{1-f^2(1-\alpha_1)(1-\alpha_2)}$$

The unknown temperatures T_1 and T_2 can be obtained from equations (D5a) and (D5b) by a trial-and-error process. Then the net rate of heat absorption by surface y can be obtained by using the conduction equation (i.e., $\dot{Q}/A=(k_2/t_2)(T_2-T_y)$).

A third application of insulation employing gaps is shown in sketch (s). For this system, there are three unknowns (T_1, T_2, and $\dot{Q}/A$, the net heat-absorption rate of surface x). Thus, three equations are needed. The first equation can be obtained by equating the heat-transfer rate

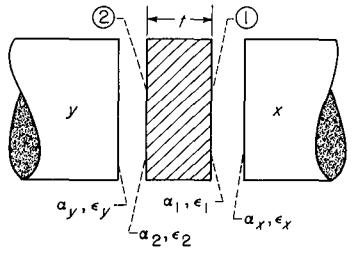

(s)

due to conduction through the insulation to the net rate of heat absorption by surface 1. This is given by

$$\frac{k}{t}(T_1-T_2)=GT_x^4+(H_1-\sigma\epsilon_1)T_1^4 \qquad \text{(D6a)}$$

where

$$G_1=\frac{\sigma\epsilon_x f\alpha_1}{1-f^2(1-\alpha_1)(1-\alpha_x)}$$

and

$$H_1=\frac{\sigma\epsilon_1 f^2(1-\alpha_x)\alpha_1}{1-f^2(1-\alpha_1)(1-\alpha_x)}$$

The next equation that can be written states that this net rate of heat absorption by surface 1 (due to thermal radiation from surface x) must be equal to the net rate of heat emission from surface 2. This is given by

$$G_1T_x^4+(H_1-\sigma\epsilon_1)T_1^4=(\sigma\epsilon_2-E_2)T_2^4-B_2T_y^4 \qquad \text{(D6b)}$$

where

$$B_2=\frac{\sigma\epsilon_y f\alpha_2}{1-f^2(1-\alpha_2)(1-\alpha_y)}$$

and

$$E_2=\frac{\sigma\epsilon_2 f^2(1-\alpha_y)\alpha_2}{1-f^2(1-\alpha_2)(1-\alpha_y)}$$

With T_1 and T_2 the only unknowns in equations (D6a) and (D6b), there are two equations with two unknowns from which T_1 and T_2 can be obtained by a trial-and-error process. Then the net rate of heat absorption by surface y is given by the third relation,

$$\frac{\dot{Q}}{A}=G_2T_2^4+(H_2-\sigma\epsilon_y)T_y^4 \qquad \text{(D6c)}$$

where

$$G_2=\frac{\sigma\epsilon_2 f\alpha_y}{1-f^2(1-\alpha_y)(1-\alpha_2)}$$

and

$$H_2=\frac{\sigma\epsilon_y f^2(1-\alpha_2)\alpha_y}{1-f^2(1-\alpha_y)(1-\alpha_2)}$$

EXTERNAL PROTECTION

Solar shadow shields.—Assuming the incoming waves of electromagnetic radiation are perpendicular to the radiation shields and that there is no temperature gradient across any particular shield, the equation for the net rate of heat absorption by surface y (sketch (t)) through one shield is given by

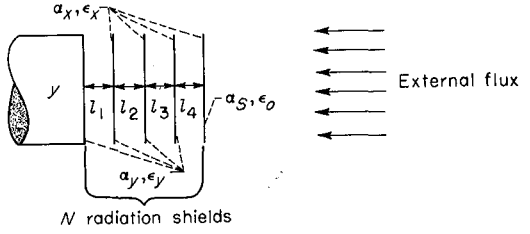

(t)

$$\left(\frac{\dot{Q}}{A}\right)_1=\underbrace{\frac{\alpha_S YG+BGT_y^4}{[\sigma(\epsilon_o+\epsilon_x)-E]}}_{D_1}+(H-\sigma\epsilon_y)T_y^4$$

For two shields,

$$\left(\frac{\dot{Q}}{A}\right)_2=\underbrace{\frac{\alpha_S YG^2+[\sigma(\epsilon_o+\epsilon_x)-E]BGT_y^4}{\{[\sigma(\epsilon_o+\epsilon_x)-E][\sigma(\epsilon_y+\epsilon_x)-E-H]-BG\}}}_{D_2}+(H-\sigma\epsilon_y)T_y^4$$

For three shields,

$$\left(\frac{\dot{Q}}{A}\right)_3=\underbrace{\frac{\alpha_S YG^3+\{[\sigma(\epsilon_o+\epsilon_x)-E][\sigma(\epsilon_y+\epsilon_x)-E-H]-BG\}BGT_y^4}{([\sigma(\epsilon_y+\epsilon_x)-E-H]\{[\sigma(\epsilon_o+\epsilon_x)-E][\sigma(\epsilon_y+\epsilon_x)-E-H]-BG\}-[\sigma(\epsilon_o+\epsilon_x)-E]BG)}}_{D_3}+(H-\sigma\epsilon_y)T_y^4$$

For $N>2$,

$$\left(\frac{\dot{Q}}{A}\right)_N=\frac{\alpha_S YG^N+(D_{N-1})BGT_y^4}{[\sigma(\epsilon_y+\epsilon_x)-E-H](D_{N-1})-(D_{N-2})BG}+(H-\sigma\epsilon_y)T_y^4 \qquad \text{(D7)}$$

where B, E, G, and H are the same as the constants for equation (D2), and Y is the incoming flux (e.g., if the incoming waves of electromagnetic radiation are from the Sun only, $Y=\sigma\epsilon_S(r_S/r_{S,P})^2\ T_S^4$). The assumption of absorptivity and emissivity of the exposed outer surface (α_S,ϵ_o) allows for solar absorptivity to be different from emissivity. These equations assume that there is heat transfer only through the end of the component and that the environmental temperature is 0° R.

A further generalization of shadow shields can be made by letting the outer shield assume a larger diameter than that of the component being protected, as shown in sketch (u). For this model, the external flux Y was assumed to be incident only on the shadow shield at the greatest distance from y.

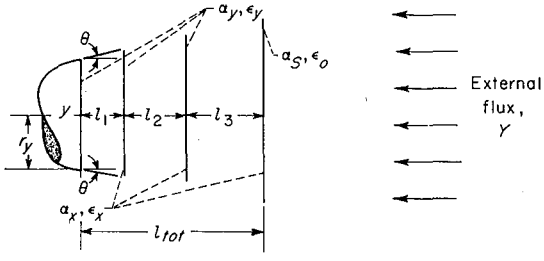

(u)

Again, in order to obtain a reasonable solution for such a shadow-shield system, it is assumed that the angle factors $f_{y,1}, f_{1,2}, f_{2,3}, \ldots$, and $f_{N-1,N}$ are all equal. This also stipulates that $f_{1,y}, f_{2,1}, \ldots$, and $f_{N,N-1}$ be equal. These conditions will be fulfilled by using the following equations for the shield radii and spacings:

$$r_N=r_y\left(1+\frac{l_1}{r_y}\tan\theta\right)^N$$

and

$$l_N=l_1\left(1+\frac{l_1}{r_y}\tan\theta\right)^{N-1}$$

where r_N is the radius of any shield in the system, l_N is the distance required between adjacent shields, and θ is half the cone angle. The total length of the shielding system (neglecting the thickness of the shields) is the sum of the individual spacings $l_1, l_2, \ldots$, and l_N. This is given by

$$l_{tot}=\sum_{i=1}^{i=N}(l_i)=\frac{-r_y}{\tan\theta}\left[1-\left(1+\frac{l_1}{r_y}\tan\theta\right)^N\right]$$

When $\theta\to 0$, $l_{tot}\to l_1(N)$.

If one shield is placed between the external heat source and the component y, the net rate of heat absorption by surface y is given by

$$\left(\frac{\dot{Q}}{A_y}\right)_1=\underbrace{\frac{GY\alpha_S\left(1+\frac{l_1}{r_y}\tan\theta\right)^2+BGT_y^4}{[\sigma(\epsilon_o+\epsilon_x)-E]}}_{D_1}+(H-\sigma\epsilon_y)T_y^4$$

where

$$B=\frac{\sigma\epsilon_y f_{y,1}\alpha_x}{1-f_{1,y}f_{y,1}(1-\alpha_x)(1-\alpha_y)}$$

$$E=\frac{\sigma\epsilon_x f_{1,y}f_{y,1}(1-\alpha_y)\alpha_x}{1-f_{1,y}f_{y,1}(1-\alpha_x)(1-\alpha_y)}$$

$$G=\frac{\sigma\epsilon_x f_{1,y}\alpha_y}{1-f_{1,y}f_{y,1}(1-\alpha_x)(1-\alpha_y)}$$

$$H=\frac{\sigma\epsilon_y f_{1,y}f_{y,1}(1-\alpha_x)\alpha_y}{1-f_{1,y}f_{y,1}(1-\alpha_x)(1-\alpha_y)}$$

and Y is the external flux. (This assumes that the waves of electromagnetic radiation from the external heat source are parallel.) With two shields,

$$\left(\frac{\dot{Q}}{A_y}\right)_2=\underbrace{\frac{G^2Y\alpha_S\left(1+\frac{l_1}{r_y}\tan\theta\right)^4+[\sigma(\epsilon_o+\epsilon_x)-E]BGT_y^4}{\{[\sigma(\epsilon_o+\epsilon_x)-E][\sigma(\epsilon_y+\epsilon_x)-E-H]-BG\}}}_{D_2}+(H-\sigma\epsilon_y)T_y^4$$

For $N>2$,

$$\left(\frac{\dot{Q}}{A_y}\right)_N=\frac{G^NY\alpha_S\left(1+\frac{l_1}{r_y}\tan\theta\right)^{2N}+(D_{N-1})BGT_y^4}{[\sigma(\epsilon_y+\epsilon_x)-E-H](D_{N-1})-BG(D_{N-2})}+(H-\sigma\epsilon_y)T_y^4$$

where D_{N-1} and D_{N-2} are the denominators of the fractions in the equations for $N-1$ and $N-2$ shields, respectively.

Solar foils.—The expression for the net rate of heat absorption by surface y through N foils can be obtained by setting the angle factor f equal to 1 in equation (D7). The resulting equation is

$$\left(\frac{\dot{Q}}{A}\right)_N = \frac{\frac{\alpha_S}{\epsilon_o}\left[\left(\frac{\alpha}{\epsilon}\right)_y\left(\frac{\epsilon}{\alpha}\right)_x\right]^N \epsilon_y Y - \sigma\epsilon_y T_y^4}{\left(1-\alpha_y+\frac{\alpha_y}{\alpha_x}\right)\left\{\frac{1-\left[\left(\frac{\alpha}{\epsilon}\right)_y\left(\frac{\epsilon}{\alpha}\right)_x\right]^N}{1-\left(\frac{\alpha}{\epsilon}\right)_y\left(\frac{\epsilon}{\alpha}\right)_x}\right\}+\frac{\epsilon_y}{\epsilon_o}\left[\left(\frac{\alpha}{\epsilon}\right)_y\left(\frac{\epsilon}{\alpha}\right)_x\right]^N} \tag{D8}$$

When $(\alpha/\epsilon)_y(\epsilon/\alpha)_x=1$, the expression

$$\left\{1-\left[\left(\frac{\alpha}{\epsilon}\right)_y\left(\frac{\epsilon}{\alpha}\right)_x\right]^N\right\}\Big/\left[1-\left(\frac{\alpha}{\epsilon}\right)_y\left(\frac{\epsilon}{\alpha}\right)_x\right]$$

should be replaced by N. This equation gives the heat-transfer rate through the end of the tank only. It was assumed that the flux Y was incident only upon the outer surface of the first shield.

Planetary shadow shields.—The expression for the heat-transfer rate (through the end of the cylinder only) and shield temperatures for the arrangement in sketch (v)

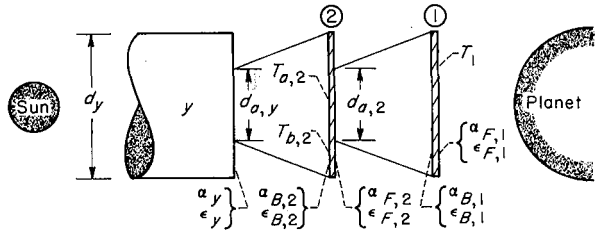

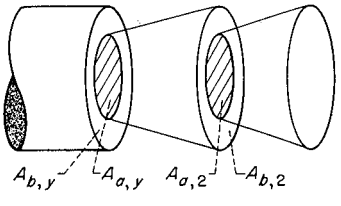

(v)

are given by

$$\frac{\dot{Q}}{A_y}=\sigma\left[\left(C_{17}+C_{18}\frac{g}{h}\right)\left(\frac{ae-bh}{ch-ag}\right)+C_{18}\frac{e}{h}+\left(C_{19}-C_{21}\right)T_y^4+C_{20}\right] \tag{D9}$$

$$T_{b,2}=\left(\frac{ae-bh}{ch-ag}\right)^{1/4}$$

$$T_{a,2}=\left[\left(\frac{ae-bh}{ch-ag}\right)\frac{g}{h}+\frac{e}{h}\right]^{1/4}$$

and

$$T_1=\left(\frac{C_1+C_5+C_3T_{b,2}^4+C_4T_{a,2}^4}{C_6-C_2}\right)^{1/4}$$

where

$$a=C_{16}-C_9-C_{12}-\left(\frac{C_4C_7}{C_6-C_2}\right)$$

$$b=C_{14}T_y^4+C_{10}+C_{11}+\left(\frac{C_1+C_5}{C_6-C_2}\right)C_7$$

$$c=\frac{C_3C_7}{C_6-C_2}+C_8+C_{13}-C_{15}$$

$$e=b-C_{10}+C_{22}$$

$$g=c+C_{15}$$

and

$$h=C_{16}\left(\frac{A_y}{A_{a,2}}\right)-C_9-C_{12}-\left(\frac{C_4C_7}{C_6-C_2}\right)$$

The expressions for the constants are shown at the end of this section. It has been assumed for these planetary shadow-shield expressions that (1) the temperature gradient through any shield normal to the shield surface is zero, (2) the tank and shields have equal diameters and are equal distances apart, (3) the cylindrical axis of the components lies on the Sun-planet axis, (4) thermal equilibrium prevails, and (5) the angle factor between a shield and space is equal to 1 minus the angle factor between shields.

Solar shadow shields near planet on Sun-planet axis.—Similarly, the expressions for the net rate of heat absorption by surface y and the

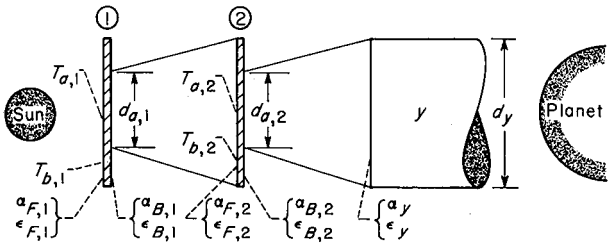

(w)

shield temperatures for the arrangement in sketch (w) are given by

$$\frac{\dot{Q}}{A_y}=\sigma\left\{\frac{C_{17}[(p-mw)(o+mi)+(n+mw)(u+mi)]+C_{18}[(u+mi)(q-mj)+(v+mj)(o+mi)]}{(p-mw)(q-mj)-(v+mj)(n+mw)}+(C_{19}-C_{21})T_y^4+C_{33}\right\} \quad \text{(D10)}$$

$$T_{b,2}=\left[\frac{(p-mw)(o+mi)+(n+mw)(u+mi)}{(p-mw)(q-mj)-(v+mj)(n+mw)}\right]^{1/4}$$

$$T_{a,2}=\left[\frac{(u+mi)(q-mj)+(v+mj)(o+mi)}{(p-mw)(q-mj)-(v+mj)(n+mw)}\right]^{1/4}$$

$$T_{b,1}=(i+jT_{b,2}^4+wT_{a,2}^4)^{1/4}$$

$$T_{a,1}=\left(\frac{C_{24}T_{b,1}^4+C_3T_{b,2}^4+C_4T_{a,2}^4+C_{23}+C_{34}}{C_{27}\dfrac{A_y}{A_{a,1}}-C_{25}}\right)^{1/4}$$

where

$$i=\frac{C_{23}+C_{26}+s(C_{23}+C_{34})}{C_{28}-C_{24}(1+s)}$$

$$j=\frac{C_3(1+s)}{C_{28}-C_{24}(1+s)}$$

$$m=C_{29}+C_{24}x$$

$$n=C_9+C_{12}-C_{16}+C_4x$$

$$o=C_{14}T_y^4+C_{31}+C_{32}+x(C_{34}+C_{23})$$

$$p=C_{16}\frac{A_y}{A_{a,2}}-C_{12}-C_9-C_4x$$

$$q=C_{15}-C_8-C_{13}-C_3x$$

$$s=\frac{C_{25}-C_{27}}{C_{27}\dfrac{A_y}{A_{a,1}}-C_{25}}$$

$$u=C_{31}+C_{35}+C_{14}T_y^4+x(C_{34}+C_{23})$$

$$v=C_8+C_{13}+C_3x$$

$$w=\frac{C_4(1+s)}{C_{28}-C_{24}(1+s)}$$

$$x=\frac{C_{30}}{C_{27}\left(\dfrac{A_y}{A_{a,1}}\right)-C_{25}}$$

Solar shadow shields near planet on planet radius normal to Sun-planet axis.—The expressions for the net heat-transfer rate through the

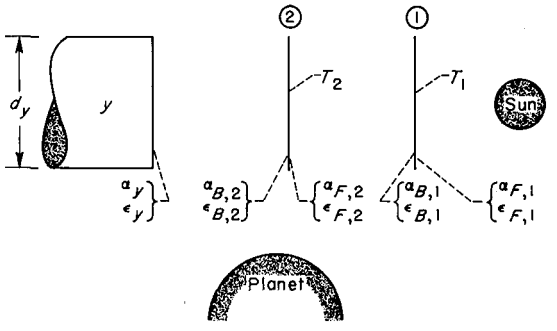

(x)

end of the cylindrical tank and shield temperatures for the arrangement shown in sketch (x) are given by

$$\frac{\dot{Q}}{A_y}=\sigma\left\{C_{44}\left[\frac{C_7(C_{36}+C_{37})+(C_6-C_2)(C_{14}T_y^4+C_{40}+C_{41})}{(C_6-C_2)(C_{42}-C_{39}-C_{45})-C_7C_{38}}\right]+C_{43}+(C_{19}-C_{21})T_y^4\right\} \quad \text{(D11)}$$

$$T_2=\left[\frac{C_7(C_{36}+C_{37})+(C_6-C_2)(C_{14}T_y^4+C_{40}+C_{41})}{(C_6-C_2)(C_{42}-C_{39}-C_{45})-C_7C_{38}}\right]^{1/4}$$

$$T_1=\left(\frac{C_{36}+C_{37}+C_{38}T_2^4}{C_6-C_2}\right)^{1/4}$$

The expressions for these constants are given at the end of this section. The preceding equations assume that (1) the temperature gradient through any shield is zero, (2) the tank and shields have equal diameters and are equal distances apart, (3) planetary flux is reflected only once before passing into space, (4) the vehicle lies in a plane perpendicular to the Sun-planet axis with the

shadow shields oriented towards the Sun, and (5) thermal equilibrium prevails.

The expressions for the constants used in this section are as follows:

$$C_1=f_{F1,P}\alpha_{F,1}C_{46}+\epsilon_s(1-f_{F1,P})\alpha_{F,1}T_s^4$$

$$C_2=\frac{\epsilon_{B,1}f_{1,2}f_{2,1}(1-\alpha_{F,2})\alpha_{B,1}}{C_{47}}$$

$$C_3=\frac{\epsilon_{F,2}\left(\frac{A_{b,2}}{A_y}\right)f_{b2,1}\alpha_{B,1}}{C_{47}}$$

$$C_4=\frac{\epsilon_{F,2}\left(\frac{A_{a,2}}{A_y}\right)f_{a2,1}\alpha_{B,1}}{C_{47}}$$

$$C_5=\frac{\epsilon_s(1-f_{2,1})f_{2,1}(1-\alpha_{F,2})\alpha_{B,1}T_s^4+\epsilon_s(1-f_{1,2})\alpha_{B,1}T_s^4}{C_{47}}+\frac{\left(\frac{A_{b,2}}{A_y}\right)f_{F2,P}f_{2,1}(1-\alpha_{F,2})\alpha_{B,1}C_{46}}{C_{47}}$$

$$C_6=\epsilon_{F,1}+\epsilon_{B,1}$$

$$C_7=\frac{\epsilon_{B,1}f_{1,2}\alpha_{F,2}}{C_{47}}$$

$$C_8=\frac{\epsilon_{F,2}\left(\frac{A_{b,2}}{A_y}\right)f_{b2,1}f_{1,2}(1-\alpha_{B,1})\alpha_{F,2}}{C_{47}}$$

$$C_9=\frac{\epsilon_{F,2}\left(\frac{A_{a,2}}{A_y}\right)f_{a2,1}f_{1,2}(1-\alpha_{B,1})\alpha_{F,2}}{C_{47}}$$

$$C_{10}=\frac{[\epsilon_s(1-f_{2,1})\alpha_{F,2}+\epsilon_s(1-f_{1,2})f_{1,2}(1-\alpha_{B,1})\alpha_{F,2}]T_s^4}{C_{47}}+\frac{\left(\frac{A_{b,2}}{A_y}\right)f_{F2,P}\alpha_{F,2}C_{46}}{C_{47}}$$

$$C_{11}=\frac{\left(\frac{A_{b,y}}{A_y}\right)f_{y,P}f_{y,2}(1-\alpha_y)\alpha_{B,2}C_{46}}{C_{48}}+\frac{[\epsilon_s(1-f_{2,y})\alpha_{B,2}+\epsilon_s(1-f_{y,2})f_{y,2}(1-\alpha_y)\alpha_{B,2}]T_s^4}{C_{48}}$$

$$C_{12}=\frac{\epsilon_{B,2}\left(\frac{A_{a,2}}{A_y}\right)f_{a2,y}f_{y,2}(1-\alpha_y)\alpha_{B,2}}{C_{48}}$$

$$C_{13}=\frac{\epsilon_{B,2}\left(\frac{A_{b,2}}{A_y}\right)f_{b2,y}f_{y,2}(1-\alpha_y)\alpha_{B,2}}{C_{48}}$$

$$C_{14}=\frac{\epsilon_y f_{y,2}\alpha_{B,2}}{C_{48}}$$

$$C_{15}=(\epsilon_{F,2}+\epsilon_{B,2})\left(\frac{A_{b,2}}{A_y}\right)$$

$$C_{16}=(\epsilon_{F,2}+\epsilon_{B,2})\left(\frac{A_{a,2}}{A_y}\right)$$

$$C_{17}=\frac{\epsilon_{B,2}\left(\frac{A_{b,2}}{A_y}\right)f_{b2,y}\alpha_y}{C_{48}}$$

$$C_{18}=\frac{\epsilon_{B,2}\left(\frac{A_{a,2}}{A_y}\right)f_{a2,y}\alpha_y}{C_{48}}$$

$$C_{19}=\frac{\epsilon_y f_{2,y}f_{y,2}(1-\alpha_{B,2})\alpha_y}{C_{48}}$$

$$C_{20}=\frac{[\epsilon_s(1-f_{y,2})\alpha_y+\epsilon_s(1-f_{2,y})f_{2,y}(1-\alpha_{B,2})\alpha_y]T_s^4}{C_{48}}+\frac{\left(\frac{A_{b,y}}{A_y}\right)f_{Fy,P}\alpha_y C_{46}}{C_{48}}$$

$$C_{21}=\epsilon_y$$

$$C_{22}=\frac{[\epsilon_s(1-f_{1,2})f_{1,2}(1-\alpha_{B,1})\alpha_{F,2}+\epsilon_s(1-f_{2,1})\alpha_{F,2}]T_s^4}{C_{47}}+\frac{\left(\frac{A_{b,2}}{A_y}\right)f_{F2,P}f_{1,2}f_{2,1}(1-\alpha_{F,2})(1-\alpha_{B,1})\alpha_{F,2}C_{46}}{C_{47}}$$

$$C_{23}=f_{F1,s}\alpha_{F,1}\left[\epsilon_s T_s^4+\epsilon_S\left(\frac{r_S}{r_{S,P}}\right)^2 T_S^4\right]$$

$$C_{24}=\frac{\epsilon_{B,1}\left(\frac{A_{b,1}}{A_y}\right)f_{b1,2}f_{2,1}(1-\alpha_{F,2})\alpha_{B,1}}{C_{47}}$$

$$C_{25}=\frac{\epsilon_{B,1}\left(\frac{A_{a,1}}{A_y}\right)f_{a1,2}f_{2,1}(1-\alpha_{F,2})\alpha_{B,1}}{C_{47}}$$

$$C_{26}=\frac{[\epsilon_s(1-f_{2,1})f_{2,1}(1-\alpha_{F,2})\alpha_{B,1}+\epsilon_s(1-f_{1,2})\alpha_{B,1}]T_s^4}{C_{47}}+\frac{\left(\frac{A_{b,1}}{A_y}\right)f_{b1,P}\alpha_{B,1}C_{46}}{C_{47}}$$

$$C_{27}=\left(\frac{A_{a,1}}{A_y}\right)(\epsilon_{F,1}+\epsilon_{B,1})$$

$$C_{28}=\left(\frac{A_{b,1}}{A_y}\right)(\epsilon_{F,1}+\epsilon_{B,1})$$

$$C_{29}=\frac{\epsilon_{B,1}\left(\frac{A_{b,1}}{A_y}\right)f_{b1,2}\alpha_{F,2}}{C_{47}}$$

$$C_{30}=\frac{\epsilon_{B,1}\left(\frac{A_{a,1}}{A_y}\right)f_{a1,2}\alpha_{F,2}}{C_{47}}$$

$$C_{31}=\frac{[\epsilon_s(1-f_{2,1})\alpha_{F,2}+\epsilon_s(1-f_{1,2})f_{1,2}(1-\alpha_{B,1})\alpha_{F,2}]T_s^4}{C_{47}}+\frac{\left(\frac{A_{b,1}}{A_y}\right)f_{b1,P}f_{1,2}(1-\alpha_{B,1})\alpha_{F,2}C_{46}}{C_{47}}$$

$$C_{32}=\frac{[\epsilon_s(1-f_{2,y})\alpha_{B,2}+\epsilon_s(1-f_{y,2})f_{y,2}(1-\alpha_y)\alpha_{B,2}]T_s^4}{C_{48}}+\frac{\left(\frac{A_{b,2}}{A_y}\right)f_{b2,P}\alpha_{B,2}C_{46}}{C_{48}}$$

$$C_{33}=\frac{[\epsilon_s(1-f_{y,2})\alpha_y+\epsilon_s(1-f_{2,y})f_{2,y}(1-\alpha_{B,2})\alpha_y]T_s^4}{C_{48}}+\frac{\left(\frac{A_{b,2}}{A_y}\right)f_{b2,P}f_{2,3}(1-\alpha_{B,2})\alpha_yC_{46}}{C_{48}}$$

$$C_{34}=\frac{[\epsilon_s(1-f_{2,1})f_{2,1}(1-\alpha_{F,2})\alpha_{B,1}+\epsilon_s(1-f_{1,2})\alpha_{B,1}]T_s^4}{C_{47}}+\frac{\left(\frac{A_{b,1}}{A_y}\right)f_{b1,P}\alpha_{B,1}f_{1,2}f_{2,1}(1-\alpha_{B,1})(1-\alpha_{F,2})C_{46}}{C_{47}}$$

$$C_{35}=\frac{[\epsilon_s(1-f_{2,y})(\alpha_{B,2})+\epsilon_s(1-f_{y,2})f_{y,2}(1-\alpha_y)\alpha_{B,2}]T_s^4}{C_{48}}+\frac{\left(\frac{A_{b,2}}{A_y}\right)f_{b2,P}f_{2,y}f_{y,2}\alpha_{B,2}(1-\alpha_{B,2})(1-\alpha_y)C_{46}}{C_{48}}$$

$$C_{36}=\epsilon_s\alpha_{F,1}T_s^4+\frac{\epsilon_s\alpha_{B,1}T_s^4[(1-f_{1,2})+(1-f_{1,2})f_{2,1}(1-\alpha_{F,2})]}{C_{47}}+f_v(\alpha_{B,1}+\alpha_{F,1})\delta$$

$$C_{37}=\epsilon_s\left(\frac{r_S}{r_{S,P}}\right)^2T_S^4{}_2\alpha_{B,1}$$

$$C_{38}=\frac{\epsilon_{F,2}f_{2,1}\alpha_{B,1}}{C_{47}}$$

$$C_{39}=\frac{\epsilon_{F,2}f_{1,2}f_{2,1}(1-\alpha_{B,1})\alpha_{F,2}}{C_{47}}$$

$$C_{40}=\frac{\epsilon_s\alpha_{F,2}T_s^4[(1-f_{2,1})+(1-f_{1,2})f_{1,2}(1-\alpha_{B,1})]}{C_{47}}+f_v\alpha_{F,2}C_{46}$$

$$C_{41}=\frac{\epsilon_s\alpha_{B,2}T_s^4[(1-f_{2,y})+(1-f_{2,y})f_{y,2}(1-\alpha_y)]}{C_{48}}+f_v\alpha_{B,2}C_{46}$$

$$C_{42}=\epsilon_{B,2}+\epsilon_{F,2}$$

$$C_{43}=\frac{\epsilon_s\alpha_yT_s^4[(1-f_{y,2})+(1-f_{2,y})f_{2,y}(1-\alpha_{B,2})]}{C_{48}}+f_v\alpha_yC_{46}$$

$$C_{44}=\frac{\epsilon_{B,2}f_{2,y}\alpha_y}{C_{48}}$$

$$C_{45}=\frac{\epsilon_{B,2}f_{2,y}f_{y,2}(1-\alpha_y)\alpha_{B,2}}{C_{48}}$$

$$C_{46}=\frac{\delta}{\sigma}=\epsilon_PT_P^4+a_P\epsilon_S\left(\frac{r_S}{r_{S,P}}\right)^2T_S^4{}_2$$

$$C_{47}=1-f_{1,2}f_{2,1}(1-\alpha_{B,1})(1-\alpha_{F,2})$$

$$C_{48}=1-f_{2,y}f_{y,2}(1-\alpha_{B,2})(1-\alpha_y)$$

Insulation.—If it is assumed that there is heat transfer only through the end of the component y, the expression for the rate of heat absorption

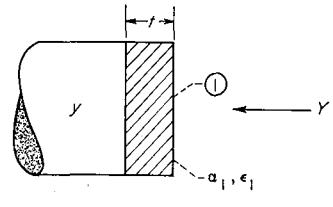

(y)

by surface y (sketch (y)) is

$$\frac{\dot{Q}}{A}=\frac{k}{t}(T_1-T_y) \qquad \text{(D12a)}$$

However, since T_1 is not known, another equation is needed. The net rate of heat absorption by

surface 1 due to thermal radiation from external sources is given by

$$\frac{\dot{Q}}{A}=\alpha_1 Y-\sigma\epsilon_1 T_1^4 \qquad \text{(D12b)}$$

These two equations can be equated (since the amount of heat that enters surface 1 must be equal to the amount of heat that passes through surface y assuming no heat loss on the edges of the insulation), and T_1 can be obtained by a trial-and-error process. After T_1 is known, either equation can be used for the heat flux.

Another application of insulation between a constant-temperature source and an external heat flux is shown in sketch (z). It is assumed that

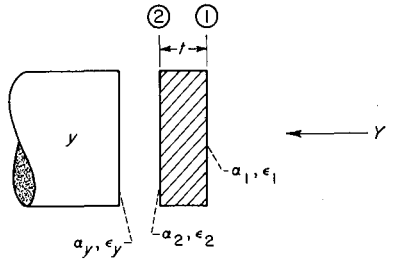

(z)

the waves of electromagnetic radiation from Y are incident only on surface 1. The net rate of heat absorption by surface 1 due to radiation from the external heat source must be equal to the conductive heat-transfer rate through the insulation. This is given by

$$\frac{k}{t}(T_1-T_2)=\alpha_1 Y-\sigma\epsilon_1 T_1^4 \qquad \text{(D13a)}$$

A similar equation can be obtained for surface 2:

$$\frac{k}{t}(T_1-T_2)=\sigma\left\{\epsilon_2 T_2^4\left[1-\frac{f_{2,y}^2(1-\alpha_y)\alpha_2}{1-f_{2,y}^2(1-\alpha_y)(1-\alpha_2)}\right]-\frac{\epsilon_y f_{2,y}\alpha_2 T_y^4}{1-f_{2,y}^2(1-\alpha_y)(1-\alpha_2)}\right\} \qquad \text{(D13b)}$$

The term on the right side of equation (D13b) is the expression for the net rate of heat emission by surface 2. If T_1 and T_2 are the only unknowns in (D13a) and (D13b), they can be obtained by a trial-and-error process. Then the rate of heat transfer into surface y is given by

$$\frac{\dot{Q}}{A}=\sigma\left\{\frac{\epsilon_2 f_{2,y}\alpha_y T_2^4}{1-f_{2,y}^2(1-\alpha_y)(1-\alpha_2)}+\epsilon_y T_y^4\left[\frac{f_{2,y}^2\alpha_y(1-\alpha_2)}{1-f_{2,y}^2(1-\alpha_y)(1-\alpha_2)}-1\right]\right\} \qquad \text{(D13c)}$$

Combining shadow shields and foils.—The heat-transfer rate for the system shown in sketch (a′) requires a trial-and-error solution between the

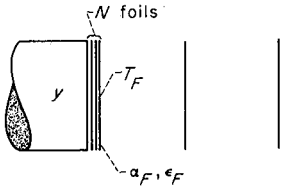

(a′)

shadow-shield equations (D9), (D10), or (D11) and the foil equation (D8). In using $\dot{Q}/A$ from the shadow-shield equations, replace T_y by T_F, α_y by α_F, and ϵ_y by ϵ_F. Then, by trial and error, the outer-foil temperature T_F is found, which gives equal values of $\dot{Q}/A$ for the shadow-shield equations and the foil equation. This method assumes that, whenever a and b areas exist on the outer foils, the outer foil has infinite conductivity laterally.

Combining shadow shields and insulation.—The heat-transfer rate for the system of shadow shields and insulation in sketch (b′) requires an

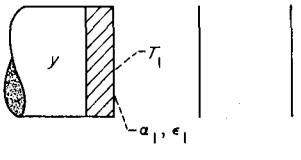

(b′)

iteration between the shadow-shield equations and the insulation equation. Again, in using $\dot{Q}/A$ from equations (D9), (D10), or (D11), it is necessary to replace T_y by T_1, ϵ_y by ϵ_1, and α_y by α_1. Then an iteration is required to determine the equilibrium value of T_1. This method also assumes that, whenever a and b areas exist on the outer surface of the insulation, this surface is assumed to have an infinite conductivity laterally.

REFERENCES

1. Kramer, John L., Lowell, Herman H., and Roudebush, William H.: Numerical Computations of Aerodynamic Heating of Liquid Propellants. NASA TN D–273, 1960.
2. Gray, V. H., Gelder, T. F., Cochran, R. P., and Goodykoontz, J. H.: Bonded and Sealed External Insulations for Liquid-Hydrogen-Fueled Rocket Tanks During Atmospheric Flight. NASA TN D–476, 1960.
3. Burry, Roger: Liquid Propellant Storage in Earth Satellite Orbits. Rocketdyne, North Am. Aviation, Inc., 1960.
4. Cramer, Kenneth R.: Orbital Storage of Cryogenic Fluids. TN 58–282, WADC, Oct. 1958.
5. Burry, R. V., and Degner, V. R.: Liquid-Propellant Storage Evaluation for Space Vehicles. Rocketdyne, North Am. Aviation, Inc., 1959.
6. Love, Charles C., Jr.: Liquid Hydrogen Transport Time Limits in Space. Paper 1087–60, Am. Rocket Soc., Inc., 1960.
7. Ehricke, Krafft A.: A Systems Analysis of Fast Manned Flights to Venus and Mars. Pt. II—Storage of Liquid and Solid Hydrogen on Nuclear Powered Interplanetary Vehicles. Paper 60–AV–1, ASME, 1960.
8. Smolak, G. R., and Knoll, R. H.: Cryogenic Propellant Storage for Round Trips to Mars and Venus. Paper 60–23, Inst. Aero. Sci., Inc., 1960.
9. Himmel, S. C., Dugan, J. F., Jr., Luidens, R. W., and Weber, R. J.: A Study of Manned Nuclear-Rocket Missions to Mars. Paper 61–49, Inst. Aerospace Sci., Inc., 1961.
10. Brun, R. J., Livingood, J. N. B., Rosenberg, E. G., and Drier, D. W.: Analysis of Liquid-Hydrogen Storage Problems for Unmanned Nuclear-Powered Mars Vehicles. NASA TN D–587, 1961.
11. Kirby, Donna Scott: Summary of Orbital and Physical Data for the Planet Mars. RM–2567, Rand Corp., Aug. 1, 1960.
12. Ambartsumyan, V. A.: Theoretical Astrophysics. Pergamon Press, 1958.
13. Jakob, Max: Heat Transfer. Vol. I. John Wiley & Sons, Inc ., 1949.
14. Scott, Russell B.: Cryogenic Engineering. D. Van Nostrand Co., Inc., 1959.
15. Gaumer, R. E., Clauss, F. J., Sibert, M. E., and Shaw, C. C.: Materials Effects in Spacecraft Thermal Control. LMSD–704019, Lockheed Aircraft Corp., Nov. 1960.
16. Gaumer, R. E.: Determination of the Effects of Satellite Environment on the Thermal Radiation Characteristics of Surfaces. Preprint 339C, SAE, 1961.
17. Schocken, Klaus: Spectral Emissivities and Solar Absorptivities. Rep. DV–TN–72–58, Army Ballistic Missile Agency, Sept. 1958.
18. Nichols, Lester D.: Effect of Shield Position and Absorptivity on Temperature Distribution of a Body Shielded from Solar Radiation in Space. NASA TN D–578, 1961.
19. Olson, O. H., Morris, J. C., Betz, H. T., and Schurin, B. D.: Determination of Emissivity and Reflectivity Data on Aircraft Structural Materials. Pt. I, Oct. 1956; pt. II and pt. II Supplement, Oct. 1958; pt. III, Jan. 1959. TR 56–222, WADC.
20. Kropschot, R. H., Schrodt, J. E., Fulk, M. M., and Hunter, B. J.: Multiple-Layer Insulation. Advances in Cryogenic Eng., vol. 5, K. D. Timmerhaus, ed., Plenum Press, Inc., 1960, pp. 189–197; discussion, pp. 197–198.
21. Hnilicka, M. P.: Engineering Aspects of Heat Transfer in Multilayer Reflective Insulation and Performance of NRC Insulation. Advances in Cryogenic Eng., vol. 5, K. D. Timmerhaus, ed., Plenum Press, Inc., 1960, pp. 199–208.
22. Riede, P. M., and Wang, D. I–J.: Characteristics and Applications of Some Superinsulations. Advances in Cryogenic Eng., vol. 5, K. D. Timmerhaus, ed., Plenum Press, Inc., 1960, pp. 209–214; discussion, pp. 214–215.
23. Bjork, R. L.: Meteoroids Versus Space Vehicles. Paper 1200–60, Am. Rocket Soc., Inc., 1960.
24. Henderson, R. E., and Stanley, P.: The Effect of Micrometeorites on Reflecting Surfaces. Paper presented at Inst. Environmental Sci., Los Angeles (Calif.), Apr. 6, 1960.
25. Lad, Robert A.: Survey of Materials Problems Resulting from Low-Pressure and Radiation Environment in Space. NASA TN D–477, 1960.
26. Kreith, Frank: Radiation Heat Transfer and Thermal Control of Spacecraft. Pub. 112, Eng. Exp. Station, Oklahoma State Univ., Apr. 1960.
27. Leuenberger, H., and Person, R. A.: Compilation of Radiation Shape Factors for Cylindrical Assemblies. Paper 56–A–144, ASME, 1956.
28. Ballinger, J. C., Elizalde, J. C., and Christensen, E. H.: Thermal Environment of Interplanetary Space. Preprint 344 B, SAE, 1961.
29. Missile and Space Vehicle Department: Space Facts. PIBD–3A, General Electric Co., May 1960.
30. De Vaucouleurs, G.: Physics of the Planet Mars. Faber and Faber (London), 1953.

TABLE I.—PLANETARY CONSTANTS

Planet	Planet temperature, T_P, °R [a]		Albedo, a_P [a]	$\epsilon_P T_P^4 + a_P \epsilon_S \left(\frac{r_S}{r_{S,P}}\right)^2 T_S^4 z$, °R^4	
	Day	Night		Day	Night
Venus	[b] 506	450(29)	[b] 0.73	3.644×10^{11}	1.107×10^{10}
Earth	[b] 525	[b] 525	[b] .39	1.433×10^{11}	4.634×10^{10}
Mars	518(29)	401(30)	.08(30)	7.501×10^{10}	2.388×10^{10}

[a] Numbers in parentheses refer to references.
[b] "Astronomical Aspects of Space Technology." Joint lecture course by Case Inst. Tech. and NASA Lewis Res. Center, Fall 1958.

U.S. GOVERNMENT PRINTING OFFICE: 1962